NACA

RESEARCH MEMORANDUM

LOW-SPEED LONGITUDINAL CHARACTERISTICS OF A CIRCULAR-ARC 52° SWEPTBACK WING OF ASPECT RATIO 2.84 WITH AND WITHOUT LEADING-EDGE AND TRAILING-EDGE FLAPS AT REYNOLDS NUMBERS FROM 1.6×10^6 TO 9.7×10^6

By Gerald V. Foster and Roland F. Griner

Langley Aeronautical Laboratory
Langley Air Force Base, Va.

NATIONAL ADVISORY COMMITTEE
FOR AERONAUTICS

WASHINGTON
August 11, 1950

NATIONAL ADVISORY COMMITTEE FOR AERONAUTICS

RESEARCH MEMORANDUM

LOW-SPEED LONGITUDINAL CHARACTERISTICS OF A CIRCULAR-ARC 52° SWEPTBACK WING OF ASPECT RATIO 2.84 WITH AND WITHOUT LEADING-EDGE AND TRAILING-EDGE FLAPS AT REYNOLDS NUMBERS FROM 1.6×10^6 TO 9.7×10^6

By Gerald V. Foster and Roland F. Griner

SUMMARY

Results of tests conducted in the Langley 19-foot pressure tunnel to determine the low-speed longitudinal characteristics of a 52° sweptback wing which had circular-arc airfoil sections and an aspect ratio of 2.84 are presented in this paper. The aerodynamic characteristics of the plain wing were investigated through a range of Reynolds numbers from 1.6×10^6 to 9.7×10^6. The effects of several spans of extensible leading-edge flaps and drooped-nose flaps on the aerodynamic characteristics of the wing were investigated. In addition, the effects of trailing-edge flaps on the wing were investigated both with and without extensible leading-edge flaps.

In the moderately low lift range, an increase in lift-curve slope and a stabilizing change in the pitching-moment curve resulted from the effects of a leading-edge vortex flow over the tip sections of the plain wing. As the angle of attack was further increased, the vortex increased in size and was shed from the wing at a point which moved progressively inboard from the tip. These changes were coincident with a decrease in slope of the lift curve and a destabilizing change of the pitching-moment curve up to the maximum lift coefficient (1.04). At the maximum lift coefficient the pitching-moment curve broke in a stable direction.

The scale effect on the aerodynamic characteristics of the wing was negligible within the range of Reynolds numbers investigated.

The addition of outboard leading-edge flaps or drooped-nose flaps which extended over the outer 25 percent of the wing semispan minimized or eliminated the initial effects of the vortex flow and provided approximately the same improvement in the stability of the wing.

Semispan split flaps increased the maximum lift coefficient of the wing from 1.04 to 1.09, whereas with extended trailing-edge flaps the maximum lift coefficient was 1.29. Neither the extended trailing-edge nor the split flaps had an appreciable effect on the stability.

The drag of the wing was high at moderate lift coefficients.

A comparison of the aerodynamic characteristics of the circular-arc wing with those of an NACA 64-series wing which had a plan form nearly identical indicates similar effects of a vortex flow. The maximum lift coefficient of the 64-series wing increased slightly with Reynolds number, but even at a Reynolds number of 11×10^6 the value of $C_{L_{max}}$ was only 0.08 larger than that of the circular-arc wing.

INTRODUCTION

As a part of a general investigation of the low-speed aerodynamic characteristics of sweptback wings being conducted in the Langley 19-foot pressure tunnel, tests have been made over a Reynolds number range from 1.6×10^6 to 9.7×10^6 of a 52° sweptback wing which had circular-arc airfoil sections and an aspect ratio of 2.84.

The longitudinal characteristics of the plain wing were obtained from force measurements and flow observations. The effects on the longitudinal stability of the wing of several spans of extensible leading-edge flaps and drooped-nose flaps were investigated. In addition, tests were made to determine the effects of trailing-edge flaps on the aerodynamic characteristics of the wing with and without extensible leading-edge flaps.

The aerodynamic characteristics of the plain wing are compared with those of a round-nose NACA 64-series wing (reference 1) which had a plan form nearly identical with that of the circular-arc wing.

SYMBOLS

C_L	lift coefficient (L/qS)
$C_{L_{max}}$	maximum lift coefficient
C_D	drag coefficient (D/qS)

C_m pitching-moment coefficient; moment about the quarter chord of mean aerodynamic chord (Moment/$q\bar{S}\bar{c}$)

C_{D_i} induced drag coefficient $\left(C_L^2/\pi A\right)$

D drag, pounds

L lift, pounds

S wing area, square feet

A aspect ratio

$\bar{c}$ mean aerodynamic chord, measured parallel to the plane of symmetry, feet $\left(\frac{2}{S}\int_0^{b/2} c^2 dy\right)$

b wing span, feet

c local chord, feet

y spanwise ordinate, feet

q free-stream dynamic pressure, pounds per square foot $\left(\frac{1}{2}\rho V^2\right)$

ρ mass density of air, slugs per cubic foot

α angle of attack of wing chord, degrees

$\alpha_{C_{L_{max}}}$ angle of attack of wing chord at $C_{L_{max}}$, degrees

V free-stream velocity, feet per second

R Reynolds number

M Mach number

δ_f trailing-edge-flap deflection, degrees

$\left(\frac{dC_m}{dC_L}\right)_{\bar{c}/4}$ variation of pitching-moment coefficient with lift coefficient with reference to the mean aerodynamic quarter chord

MODEL, TESTS, AND CORRECTIONS

Model

A plan view of the wing and some of the geometrical characteristics are given in figure 1. The wing had an aspect ratio of 2.84, a taper ratio of 0.616, and an angle of sweepback of 52.05° along a straight line connecting the leading edge of the root and theoretical tip chords. The airfoil sections of the wing normal to the line of maximum thickness (see fig. 1) were symmetrical circular-arc sections, defined by a radius of 83.26 inches, the center of which lies in a plane perpendicular to the chord line at the maximum thickness. The combined effects of circular-arc sections and taper ratio caused the leading and trailing edges to be slightly curved. The maximum thickness parallel with the plane of symmetry was 6.5 percent chord at the root and 4.1 percent chord at the tip. The wing had no geometric twist or dihedral.

The model equipped with extensible leading-edge flaps is shown in figure 2. The leading-edge flaps were of constant chord and had 37° incidence measured from the wing chord line in a plane perpendicular to a line joining the leading edges of the root and tip chords. The span of the flaps extended inboard from the 97.5-percent semispan station to the 42.5-percent semispan station. Provisions were made for several smaller spans, the smallest of which extended over the outer 15 percent of the wing semispan.

The drooped-nose flaps were investigated with spans of 0.25b/2, 0.45b/2, and 0.60b/2. The chord of these flaps was approximately 19 percent of the wing chord when it was measured parallel with the plane of symmetry of the wing. These flaps could be deflected 20°, 30°, or 40° measured as shown in figure 2.

Trailing-edge flaps of 20 percent chord, measured streamwise, were located at the 80-percent and 100-percent-chord lines (fig. 2). The flaps located at the trailing edge are referred to as "extended trailing-edge flaps," whereas those located forward are referred to as "split flaps." The angles of deflection of the flaps are given with reference to the wing lower surface, or a linear extension of the lower surface, in a plane normal to the maximum thickness line.

Tests

Figure 3 shows the wing in the test section of the Langley 19-foot pressure tunnel where the tests were conducted in an atmosphere compressed to about 33 pounds per square inch absolute. Measurements of lift, drag, and pitching moment were made through a range of angle of

attack from -4° to 32°. Tests of the plain wing were made at Reynolds numbers of 1.6×10^6, 5.9×10^6, and 9.7×10^6. The wing with flaps was tested at Reynolds numbers from 5.5×10^6 to 6.0×10^6. The Mach numbers corresponding to Reynolds numbers obtained in this investigation are as follows:

M	R
0.08	1.6×10^6
.11	5.5×10^6
.12	6.0×10^6
.19	9.7×10^6

Studies to determine, in a qualitative manner, the nature of the air flow above the wing surface were made by observing the effects of the air flow on a single tuft attached to a probe. Studies of the flow changes on the wing surface were also made by observations of tufts attached to the upper surface of the wing.

Corrections

The data are presented in nondimensional coefficient form and have been corrected for the effects of the tare and interference of model supports and air-stream misalinement. Jet-boundary corrections based on the method presented in reference 2 have been applied to the angles of attack and drag coefficients. The pitching-moment coefficients have been corrected for the distortion of the wing loading induced by the tunnel restriction.

RESULTS AND DISCUSSION

Plain Wing

Flow characteristics.- A leading-edge vortex type of flow similar to that described in references 3 and 4 was anticipated with this wing inasmuch as the wing had a sharp leading edge and was highly swept back. Probe studies indicated that, at approximately 3° angle of attack, a small vortex, approximately conical in shape, formed along the leading edge. The vortex increased in size from the root to the tip where it

was shed from the wing. As the angle of attack was increased, the size of the vortex increased and the point at which it was shed from the wing moved progressively inboard from the tip.

The results of visual observation of the effect of the air flow on surface tufts (fig. 4) show that the flow near the leading edge assumed a spanwise direction toward the tips at the same angle of attack at which the vortex flow formed. This surface outflow spread rearward at the tip sections and moved progressively inboard with increase of angle of attack. An area of stalled flow developed along the leading edge of the tip sections at 20° angle of attack, beyond which the stalled flow spreads chordwise and inward along the leading edge.

Force characteristics.- The lift, drag, and pitching-moment characteristics are presented in figure 5. Both the lift and pitching-moment curves show evidence of the effects of the vortex flow. In the low lift range up to $C_L = 0.20$, the lift curves have a linear slope of 0.049, and the pitching-moment curves indicate that the wing became slightly unstable. From $C_L = 0.20$ to $C_L \approx 0.55$ the slopes of the lift curves increase gradually to 0.071, and the variation of pitching-moment coefficients exhibits large negative slopes. These changes result from an increase of lift at the tip sections caused by the vortex flow (reference 4). Beyond $C_L \approx 0.55$, the slopes of the lift curves decrease and the pitching-moment curves up to $C_{L_{max}}$ (1.04) have positive slopes. This moment break is attributed to a forward shift of the center of pressure of the wing, caused by the effects of the increased size of the vortex over the forward portion of inboard sections of the wing and the inboard shift of the point at which the vortex was shed from the wing. Similar changes of lift and moment characteristics have been found to exist even with an NACA 64-series wing (reference 1) having a plan form nearly identical to that of the present wing (fig. 6). At $C_{L_{max}}$ the present wing had a diving tendency which is believed to result from a rearward shift of the center of pressure probably caused by the effects of the vortex flow on the rearward portion of the inboard sections of the wing; however, large values of drag occurring at the tip sections may be a large contributing factor.

The drag curves of the wing (fig. 5) depart rapidly from the variation of approximate induced drag coefficient with an increase in lift coefficient and reach high values of drag coefficient at moderate lift coefficients. A comparison of the drag characteristics of the circular-arc and NACA 64-series wing presented in figure 6 indicates that at the high Reynolds number the drag coefficients of the NACA 64-series wing more nearly approach the variation of approximate induced-drag coefficient and, consequently, are lower than the drag coefficients obtained with the circular-arc wing, particularly, at low and moderate lift coefficients. The marked difference in drag of the two wings is due to the

presence of the vortex flow at a much lower lift coefficient with the circular-arc wing than with the NACA 64-series wing.

Variation of Reynolds numbers (1.6×10^6 to 9.7×10^6) had a negligible effect on the aerodynamic characteristics of the present wing (fig. 5). In the case of the NACA 64-series wing, the lift coefficients at which the effects of the vortex flow were realized increased markedly with Reynolds number (fig. 6). The maximum lift coefficient of the NACA 64-series wing increased slightly with Reynolds number, but even at a Reynolds number of 11×10^6 the value of $C_{L_{max}}$ was only 0.08 larger than that of the circular-arc wing.

Effects of Trailing-Edge Flaps

The effects of semispan split and extended trailing-edge flaps on the aerodynamic characteristics of the wing are presented in figures 7 and 8. The results indicate that the extended trailing-edge flaps at the smallest deflection had a stabilizing tendency at high lift coefficients prior to $C_{L_{max}}$, but only a small effect at lower lift coefficients. With increase in deflection of the flaps, the stabilizing tendency in the high lift range decreased; however, the changes in stability of the basic wing in the moderate lift range were reduced. The values of $C_{L_{max}}$ obtained with various arrangements of trailing-edge flaps are summarized in the following table:

δ_f (deg)	Extended T.E. flaps	Split flaps
15	1.24	----
30	1.28	----
45	1.32	----
60	1.29	1.09
Plain wing 1.04		

Effects of Leading-Edge Flaps

The effects of variations in span of extensible leading-edge flaps and drooped-nose flaps on the aerodynamic characteristics of the wing

are presented in figures 9 to 13, and some of the more important results are summarized in table I.

The main effect of either the extensible leading-edge flaps or 0.25b/2 drooped-nose flaps was to minimize or eliminate the effects of the vortex flow on the tip sections through the moderately low lift range. Comparison of figures 4 and 10 shows that the occurrence of outflow along the leading edge at the tip was delayed with the extensible leading-edge flaps deflected. Thus, the lift increase due to the presence of a vortex flow over the tip sections of the plain wing probably was not realized when the leading-edge flaps extended over the tip sections and, consequently, the large change in the pitching-moment characteristics in the moderately low lift range was not obtained.

Figure 12 shows that the large undesirable change of the longitudinal stability parameter, $\left(\frac{dC_m}{dC_L}\right)_{\bar{c}/4}$, up to $0.85C_{L_{max}}$ of the wing was reduced from 0.33 to 0.11 with the $0.25\frac{b}{2}$-span extensible leading-edge flaps; whereas with the $0.25\frac{b}{2}$-span drooped-nose flaps deflected 30°, the change in $\left(\frac{dC_m}{dC_L}\right)_{\bar{c}/4}$ was 0.14. The effectiveness of $0.25\frac{b}{2}$-span drooped-nose flaps deflected either 20° or 40° was essentially the same as that obtained for the deflection of 30°; therefore, the data for flap deflections other than 30° are not presented. Increasing the span of the extensible leading-edge flaps from 25 percent to either 35 or 45 percent of the wing semispan resulted in no appreciable change in the stability at moderately low lift coefficients (table I); however, in the high lift range the pitching-moment curves broke in a stable direction at lift coefficients which became progressively lower with increase of flap span. This earlier stabilizing tendency may result from a greater relative lift on the outboard part of the wing with extensible leading-edge flaps of larger spans. Extensible leading-edge flaps of 0.55b/2 span and drooped-nose flaps of 0.45b/2 span and 0.60b/2 span had adverse effects on the longitudinal stability at high lift coefficients (table I).

Inasmuch as leading-edge flaps were most effective when they were limited principally to the tip sections, the influence of the root sections on the longitudinal stability of the wing was briefly investigated with a modification of the leading edges of the root sections. The modification extended from the plane of symmetry to 25 percent wing semispan and included an increase of leading-edge radii from an infinitely small value to 1/2 inch. The contours of the modified sections were faired linearly from the leading-edge radius to the original section at approximately 0.13 chord. Tests were made of the modified wing with and without extensible leading-edge flaps. No appreciable effect was realized with the wing without flaps; however, the results

with 0.25b/2 extensible leading-edge flaps indicate that the rounded leading edge caused a gradual reduction of the slope of the pitching-moment curve up to $C_L = 0.9$ (fig. 13).

Effect of Leading-Edge and Trailing-Edge Flaps in Combination

Data showing the effects of combinations of extensible leading-edge flaps and trailing-edge flaps are presented in figures 14 to 16.

Longitudinal stability.- A comparison of figures 12 and 16 indicates that the large negative increases of $\left(\frac{dC_m}{dC_L}\right)_{\bar{c}/4}$ which occurred at lift coefficients prior to $C_{L_{max}}$ with extensible leading-edge flaps were slightly delayed with the addition of trailing-edge flaps. Although the data are not presented, split flaps of 0.4 or 0.65b/2 span had practically the same effect as the 0.5b/2-span split flaps.

Maximum lift.- As may be seen in table I, values of maximum lift coefficient of the wing with combinations of leading-edge and trailing-edge flaps were larger, particularly with leading-edge flaps of large span, than would be anticipated by the individual contributions of the flaps.

Drag.- Inasmuch as the drag of the wing for all configurations with flaps deflected was high, computations have been made of the gliding and sinking speeds for power-off conditions of the wing with $0.25\frac{b}{2}$-span extensible leading-edge flaps both with and without trailing-edge flaps. The results (fig. 17) presented as contours of sinking and gliding speed (based on a wing loading of 40 lb per sq ft at sea level) have been superposed on the variations of L/D with C_L. For purposes of comparison, results are included of a 52° sweptback NACA 64-series wing (reference 5) and a 42° sweptback circular-arc wing (reference 6). The wing configurations used (fig. 17) were selected from those configurations exhibiting longitudinal stability which might be desirable at low speeds.

Although the addition of trailing-edge flaps reduced the gliding and sinking speeds of the present wing, even with the extended trailing-edge flaps deflected, the minimum sinking speed of the wing at $0.85C_{L_{max}}$ amounted to about 45 feet per second. Provided a higher gliding speed with extended trailing-edge flaps would be permissible, the maximum reduction of sinking speed would be only about 8 feet per second from that obtained at $0.85C_{L_{max}}$.

Figure 17 shows that, although extended trailing-edge flaps were effective with the present wing in reducing the sinking speed at $0.85C_{L_{max}}$, the minimum sinking speed of the present wing is about 15 feet per second greater than the sinking speeds of the other wings with split flaps deflected.

SUMMARY OF RESULTS

The results of a low-speed longitudinal stability investigation of a 52° sweptback circular-arc wing which had an aspect ratio of 2.84 indicate that:

1. In the moderately low lift range an increase in lift-curve slope and a stabilizing change in the pitching-moment curve resulted from the effects of a leading-edge vortex flow over the tip sections. As the angle of attack was further increased, the vortex increased in size and was shed from the wing at a point which moved progressively inboard from the tip. These changes were coincident with a decrease in slope of the lift curve and a destabilizing change of the pitching-moment curve up to maximum lift coefficient of 1.04. At the maximum lift coefficient the pitching-moment curve broke in a stable direction.

2. The scale effect on the aerodynamic characteristics of the wing was negligible within the range of Reynolds numbers, 1.6×10^6 to 9.7×10^6, of the tests.

3. The addition of outboard extensible leading-edge flaps or drooped-nose flaps which extended over the outer 25 percent of the wing semispan minimized or eliminated the initial effects of the vortex flow and provided approximately the same improvement in the stability of the wing.

4. Semispan split flaps increased the maximum lift coefficient of the wing from 1.04 to 1.09, whereas with extended trailing-edge flaps the maximum lift coefficient was 1.29. Neither the extended trailing-edge nor split flaps had an appreciable effect on the stability.

5. The drag of the wing was high at moderate lift coefficients.

6. A comparison of the aerodynamic characteristics of the circular-arc wing with those of an NACA 64-series wing which had a similar plan

form indicates similar effects of a vortex flow. The maximum lift coefficient of the 64-series wing increased slightly with Reynolds number, but even at a Reynolds number of 11×10^6 the value of $C_{L_{max}}$ was only 0.08 larger than that of the circular-arc wing.

Langley Aeronautical Laboratory
National Advisory Committee for Aeronautics
Langley Air Force Base, Va.

REFERENCES

1. Fitzpatrick, James E., and Foster, Gerald V.: Static Longitudinal Aerodynamic Characteristics of a 52° Sweptback Wing of Aspect Ratio 2.88 at Reynolds Numbers from 2,000,000 to 11,000,000. NACA RM L8H25, 1948.

2. Eisenstadt, Bertram J.: Boundary-Induced Upwash for Yawed and Swept-Back Wings in Closed Circular Wind Tunnels. NACA TN 1265, 1947.

3. Wilson, Herbert A., Jr., and Lovell, J. Calvin: Full-Scale Investigation of the Maximum Lift and Flow Characteristics of an Airplane Having Approximately Triangular Plan Form. NACA RM L6K20, 1947.

4. Lange, Roy H., Whittle, Edward F., Jr., and Fink, Marvin P.: Investigation at Large Scale of the Pressure Distribution and Flow Phenomena over a Wing with the Leading Edge Swept Back 47.5° Having Circular-Arc Airfoil Sections and Equipped with Drooped-Nose and Plain Flaps. NACA RM L9G15, 1949.

5. Foster, Gerald V., and Fitzpatrick, James E.: Longitudinal-Stability Investigation of High-Lift and Stall-Control Devices on a 52° Sweptback Wing with and without Fuselage and Horizontal Tail at a Reynolds Number of 6.8×10^6. NACA RM L8I08, 1948.

6. Neely, Robert H., and Koven, William: Low-Speed Characteristics in Pitch of a 42° Sweptback Wing with Aspect Ratio 3.9 and Circular-Arc Airfoil Sections. NACA RM L7E23, 1947.

TABLE I

SUMMARY OF CHARACTERISTICS OF A 52° SWEPTBACK CIRCULAR-ARC WING WITH VARIOUS FLAPS

Configuration	Flap span (b/2)	$C_{L_{max}}$	$\alpha C_{L_{max}}$	D/L at $0.85C_{L_{max}}$	C_m characteristics	Fig.
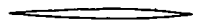	Off	1.04	24.5°	0.279	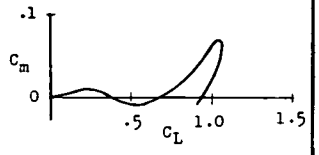	5
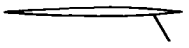	0.50	1.09	21.0°	.246	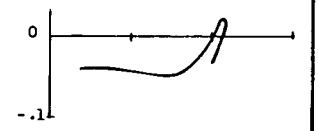	8
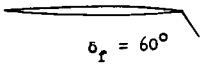 $\delta_f = 60°$	.50	1.29	22.0	.247	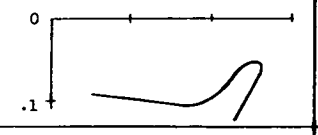	8
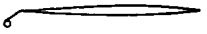	.15	1.06	26.0°	.310	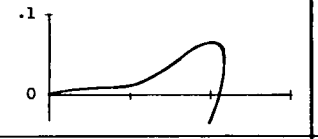	9
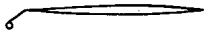	.25	1.06	27.5°	.310	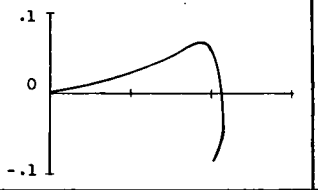	9
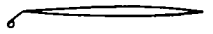	.35	1.22	[a] 31.2°	.416	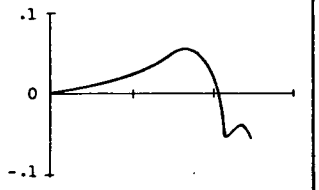	9
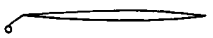	.45	1.14	28.1°	.312	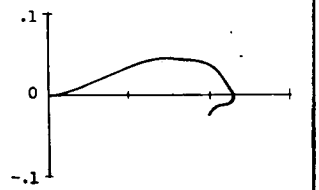	— —
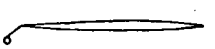	.55	1.12	27.2°	.252	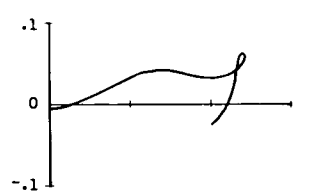	— —

[a]Maximum angle of attack tested.

TABLE I.- SUMMARY OF CHARACTERISTICS - Concluded

Configuration	Flap span (b/2)	$C_{L_{max}}$	$\alpha_{C_{L_{max}}}$	D/L at $0.85C_{L_{max}}$	C_m characteristics	Fig.
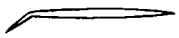	0.25	1.06	26.0°	0.321	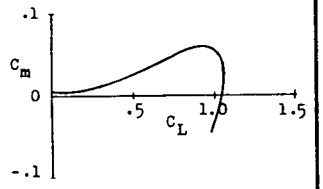	11
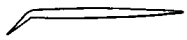	.45	1.18	29.5°	.349	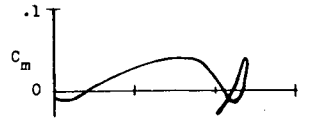	11
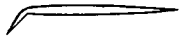	.60	1.19	29.0°	.299	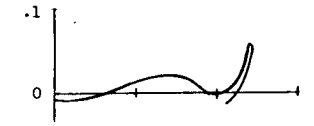	11
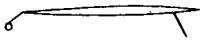	L.E. 0.25 T.E. 0.50	1.18	27.0°	.327	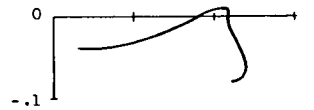	14
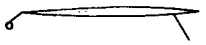	L.E. 0.55 T.E. 0.50	1.34	24.5°	.277	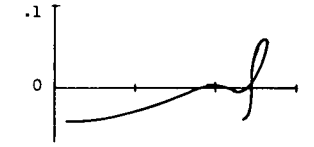	14
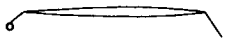 $\delta_f = 60°$	L.E. 0.25 T.E. 0.50	1.30	23.6°	.269	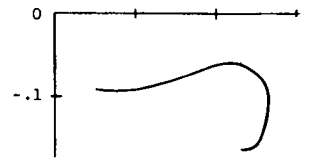	15
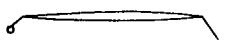 $\delta_f = 60°$	L.E. 0.55 T.E. 0.50	1.58	23.5°	.275	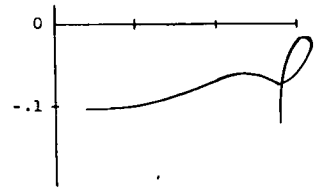	15

NACA

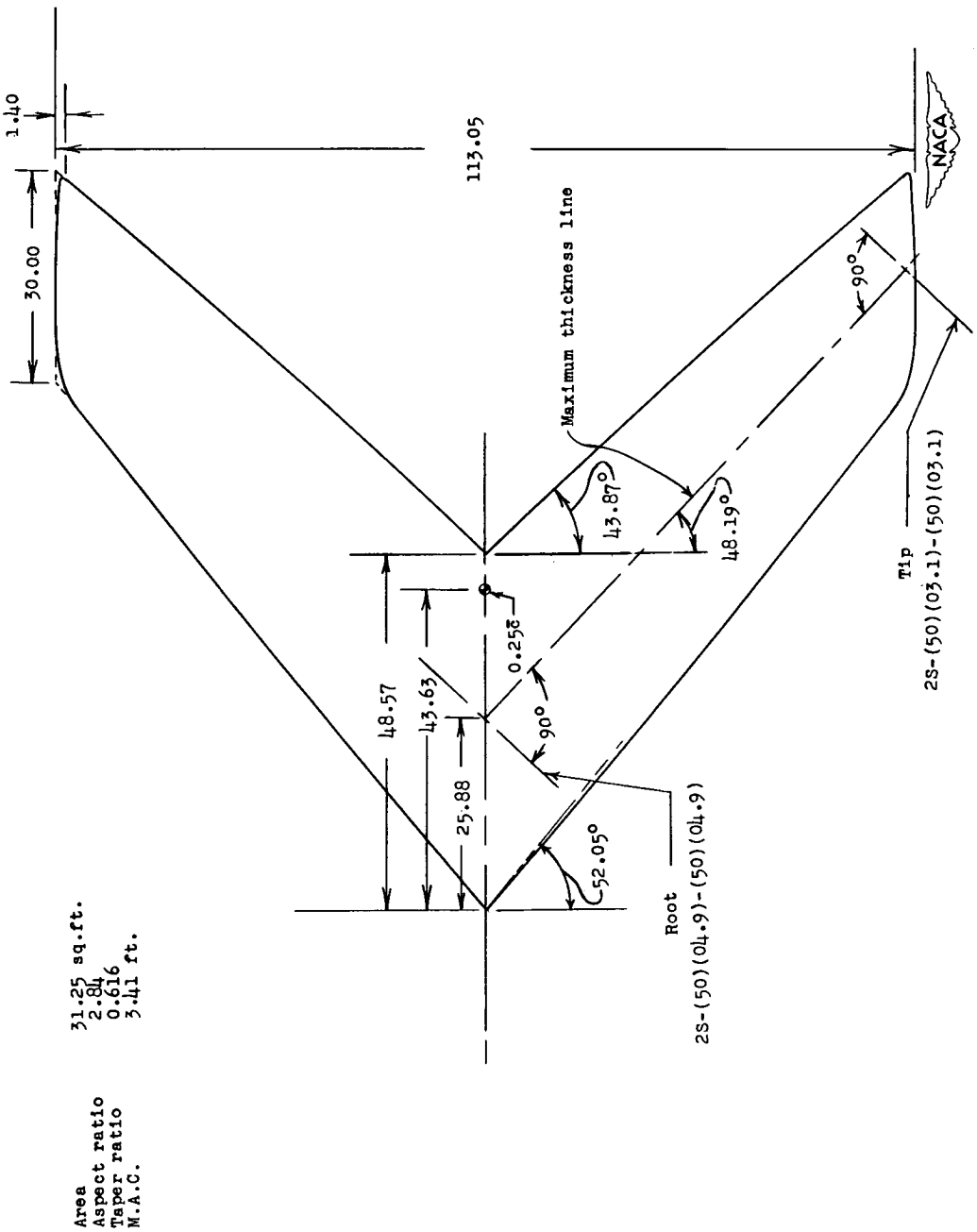

Figure 1.- Plan form of 52° sweptback wing. All dimensions given are in inches unless otherwise noted.

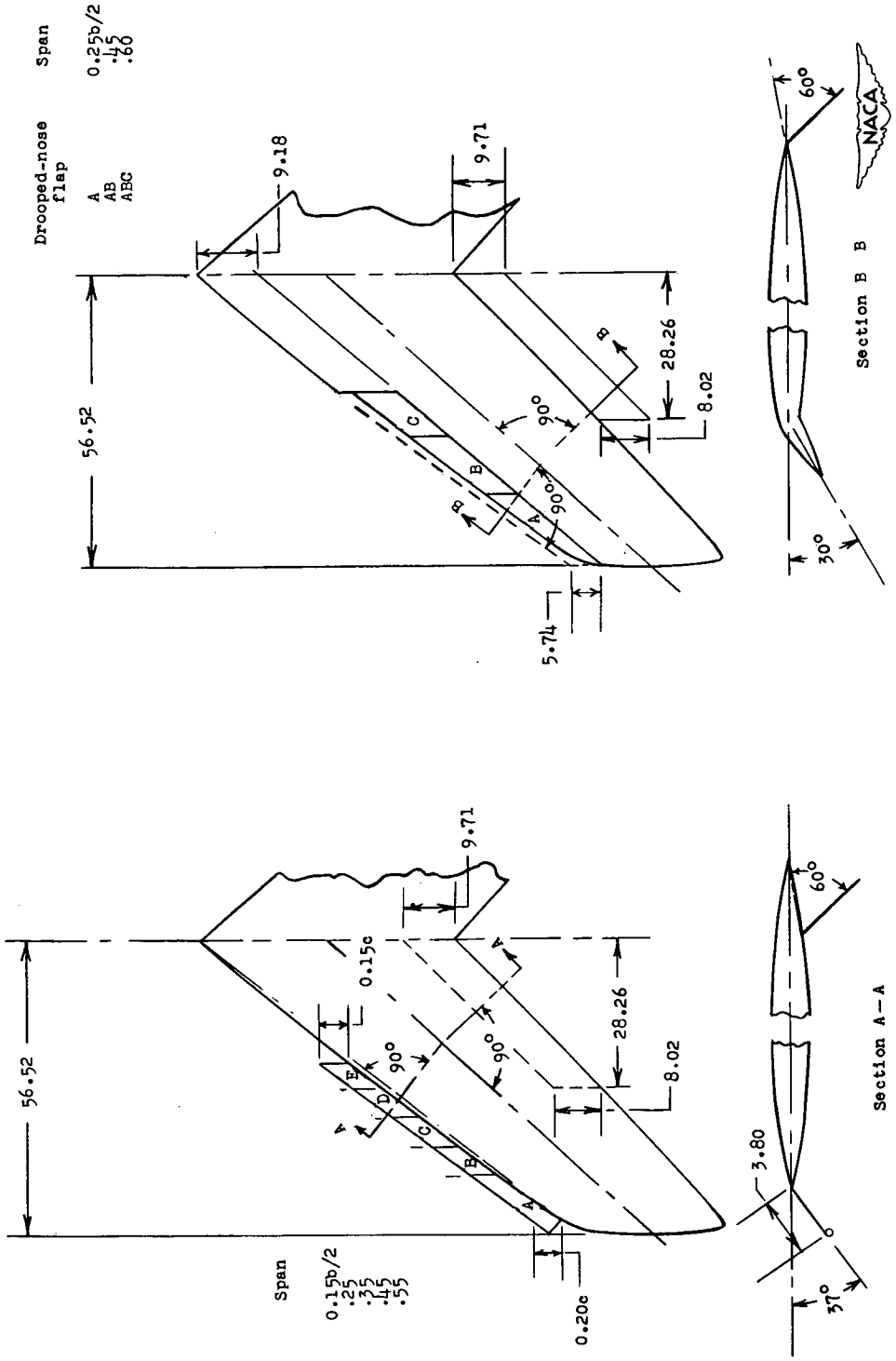

Figure 2.- Details of leading-edge and trailing-edge flaps on a 52° sweptback wing. All dimensions given are in inches unless otherwise noted.

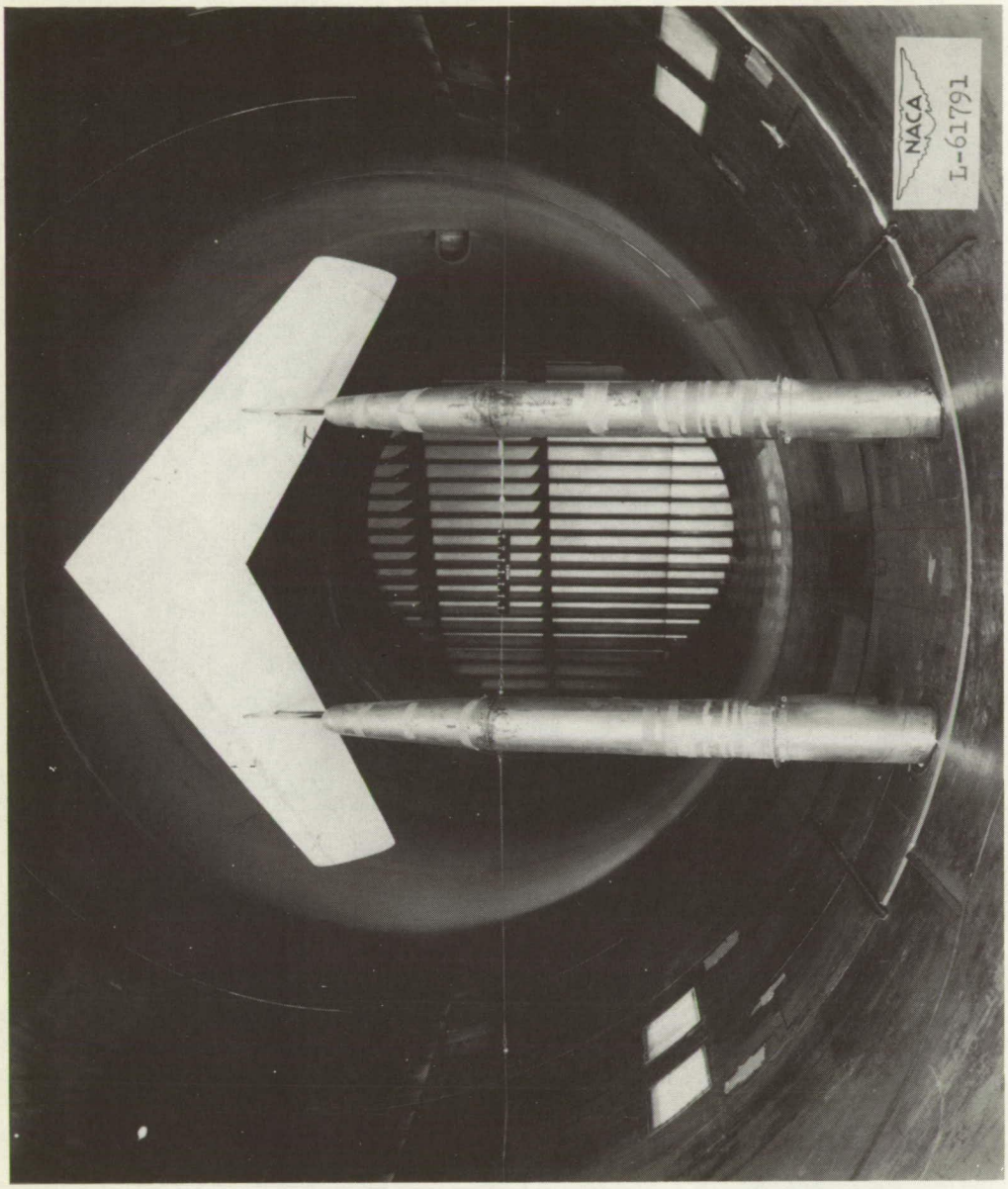

Figure 3.- The 52° sweptback wing mounted in the Langley 19-foot pressure tunnel.

Page intentionally left blank

Page intentionally left blank

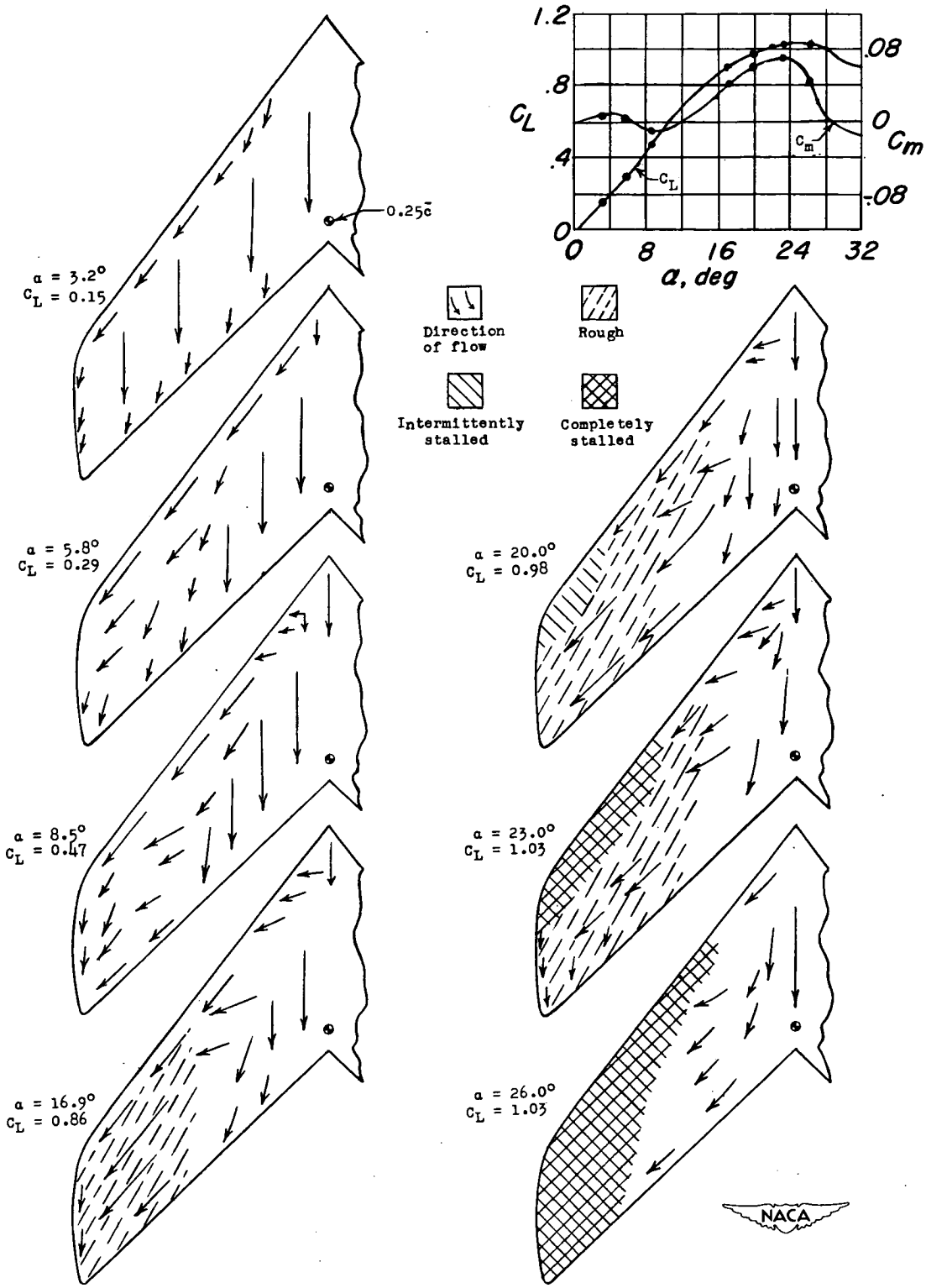

Figure 4.- Stall characteristics of a 52° sweptback wing. R = 5.9 × 10^6.

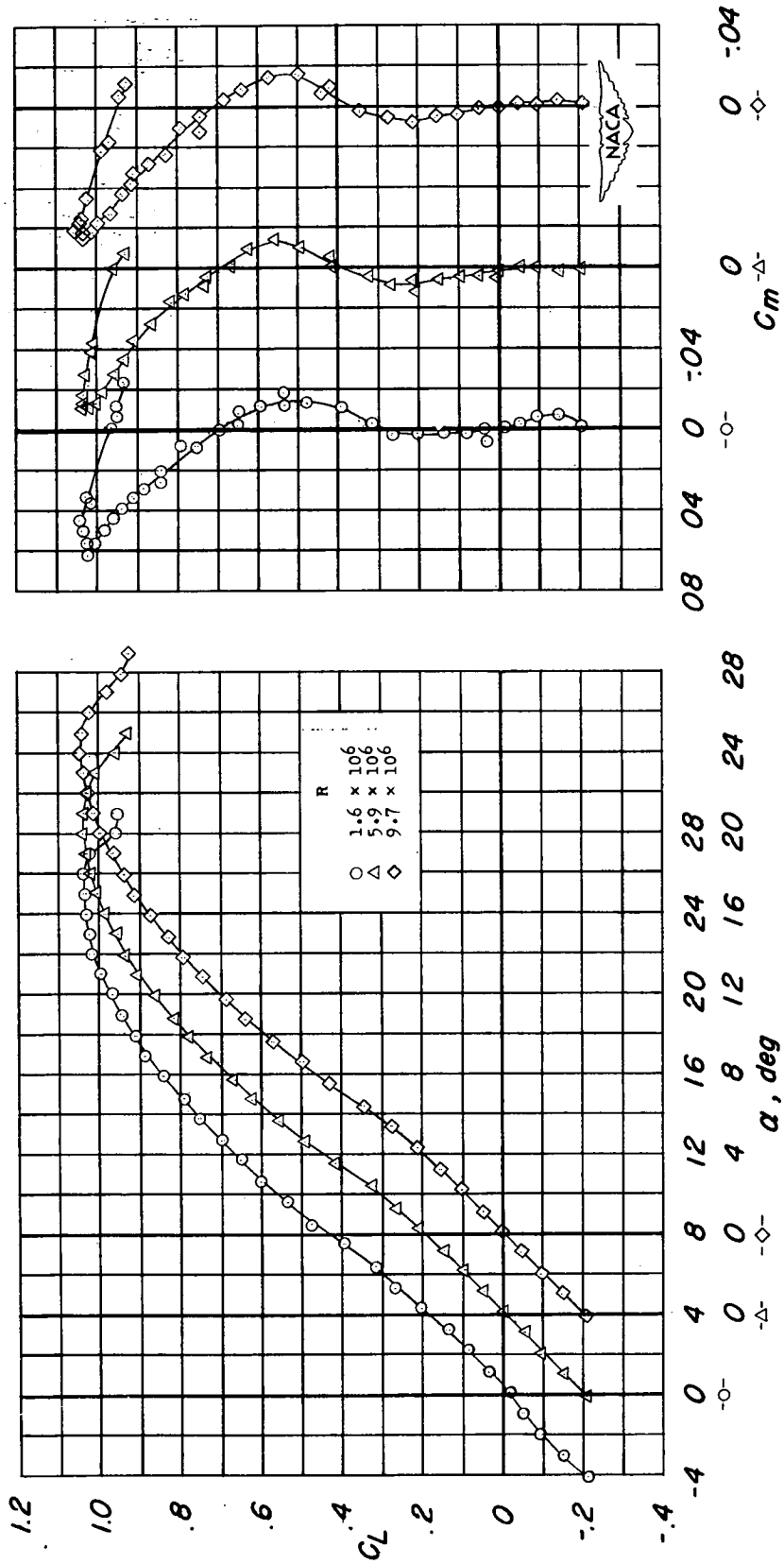

(a) C_L plotted against α and C_m.

Figure 5.- Aerodynamic characteristics of a 52° sweptback wing at several Reynolds numbers.

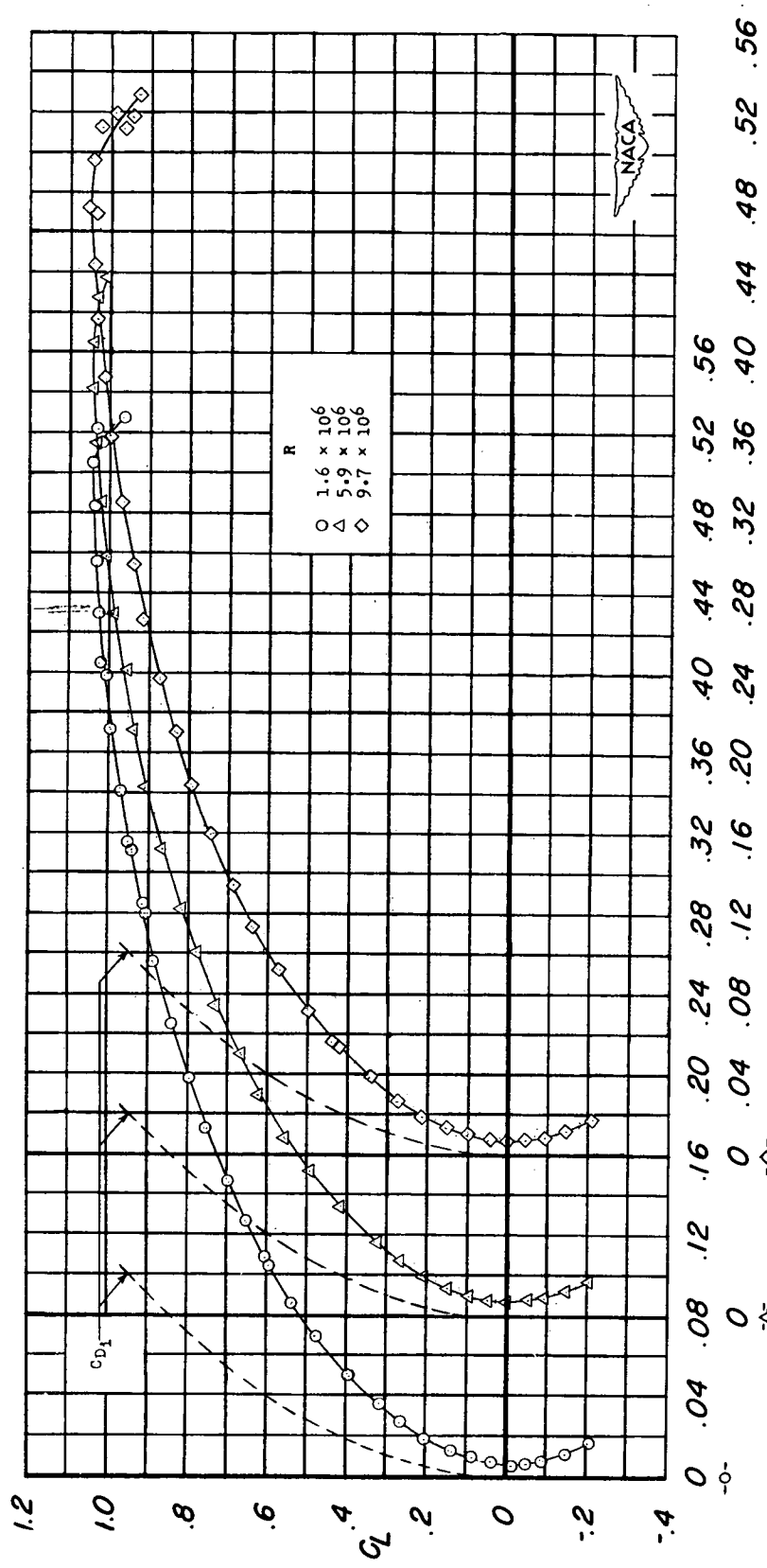

(b) C_L plotted against C_D.

Figure 5.- Concluded.

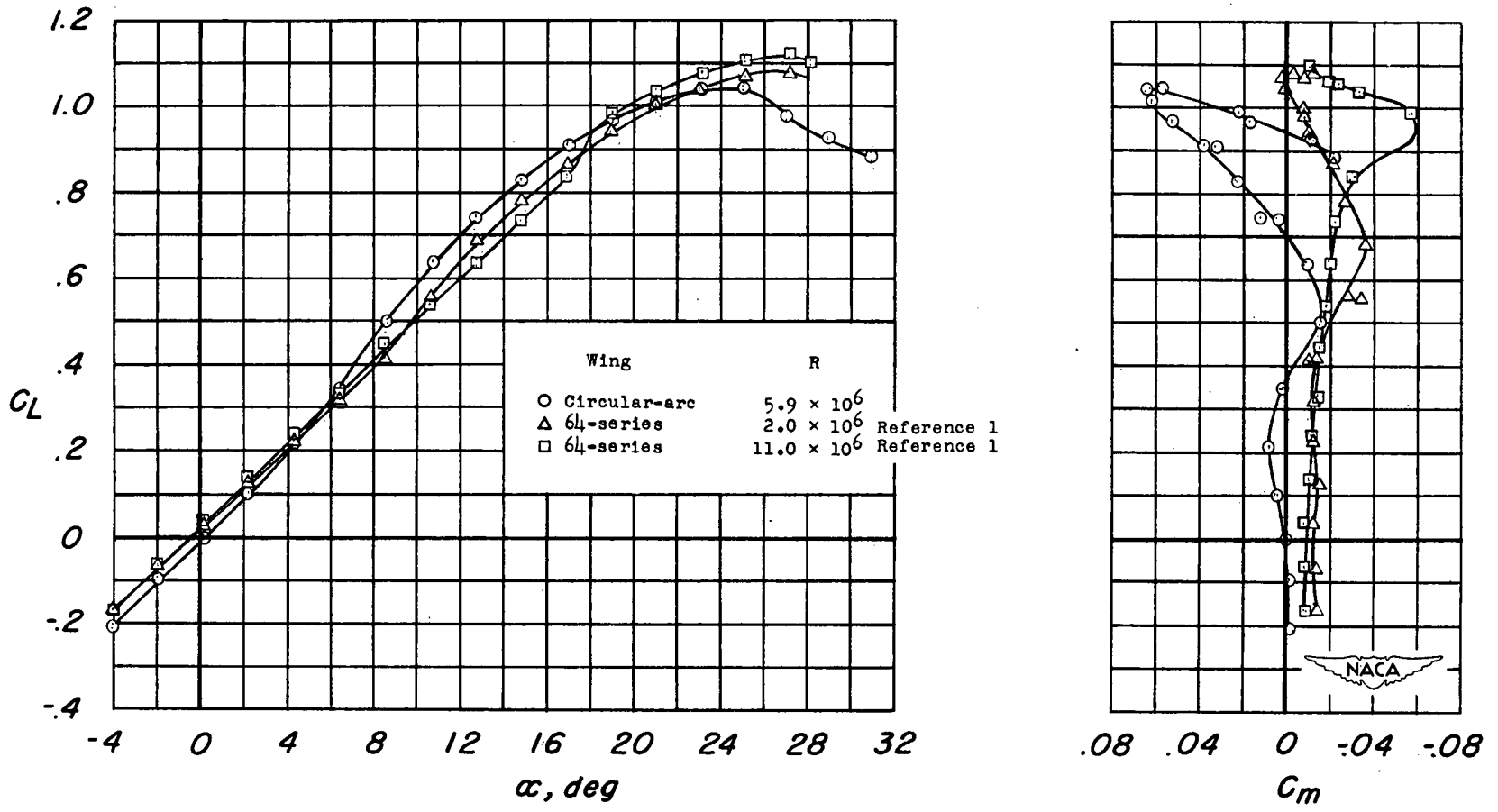

(a) C_L plotted against α and C_m.

Figure 6.- Comparison of the aerodynamic characteristics of a circular-arc wing and a 64-series wing; leading edges swept back 52°; aspect ratio approximately 2.85.

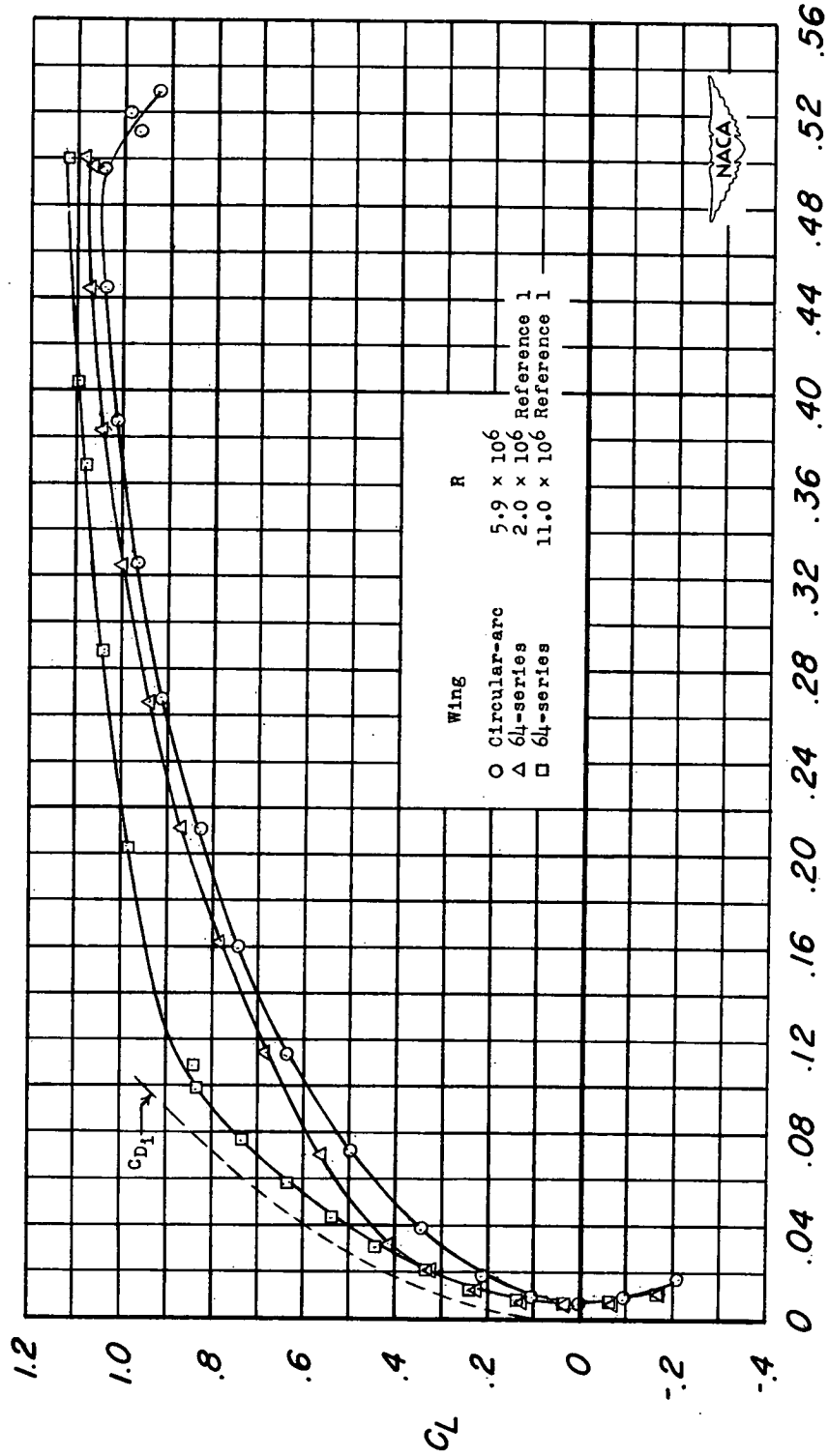

(b) C_L plotted against C_D.

Figure 6.- Concluded.

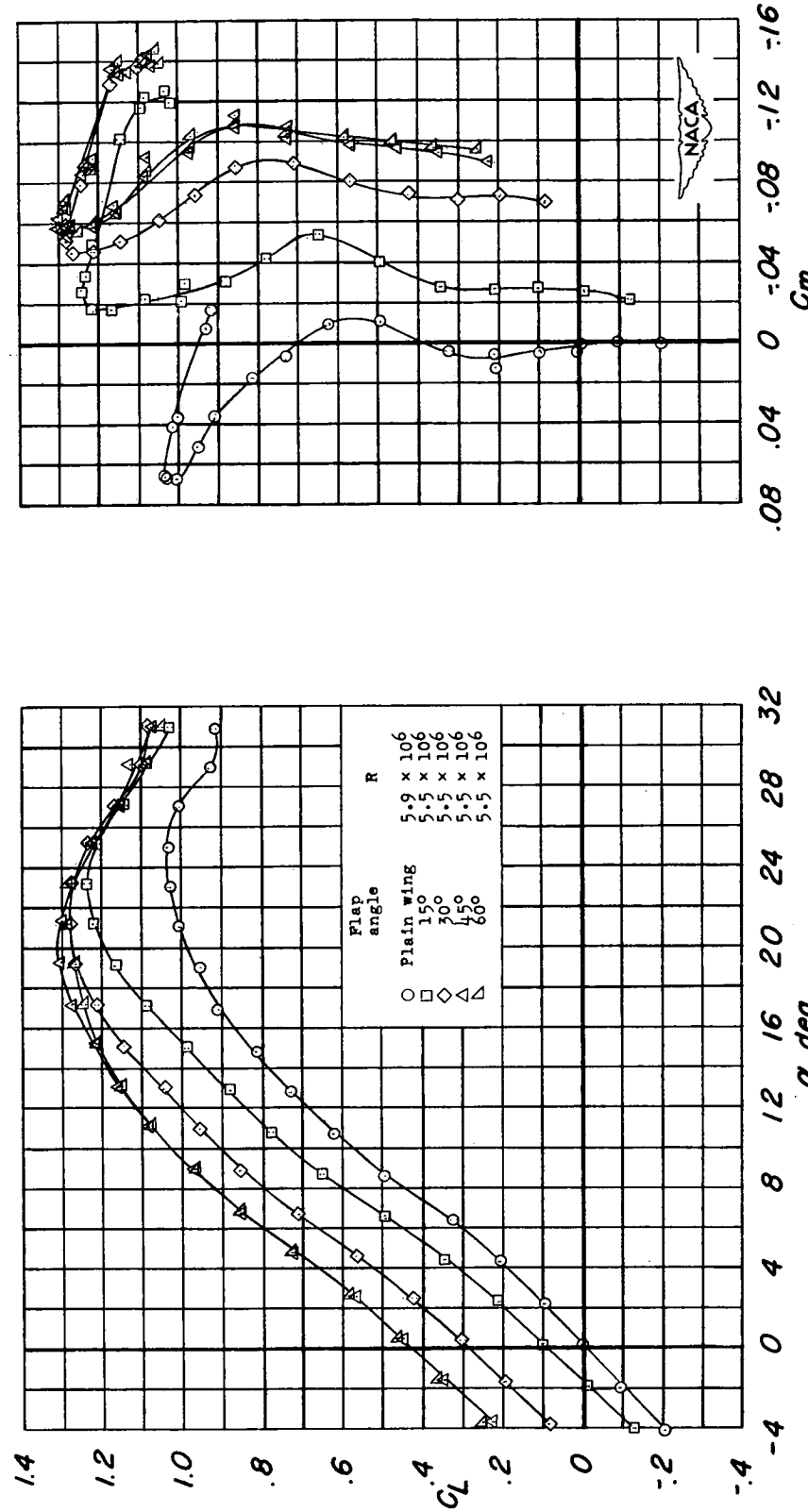

(a) C_L plotted against α and C_m.

Figure 7.- Effect of semispan extended trailing-edge flap deflection on the aerodynamic characteristics of a 52° sweptback wing.

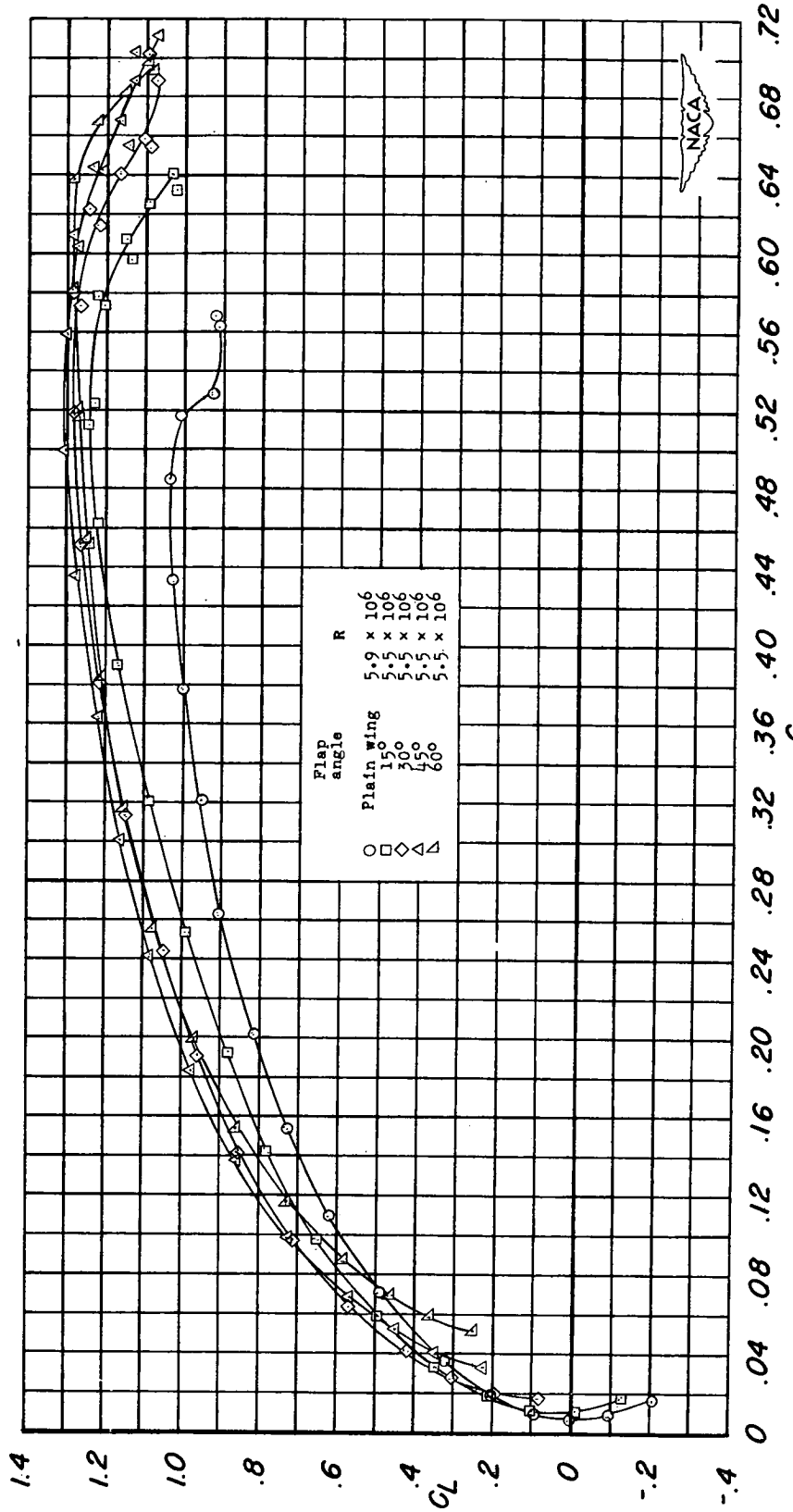

(b) C_L plotted against C_D.

Figure 7.- Concluded.

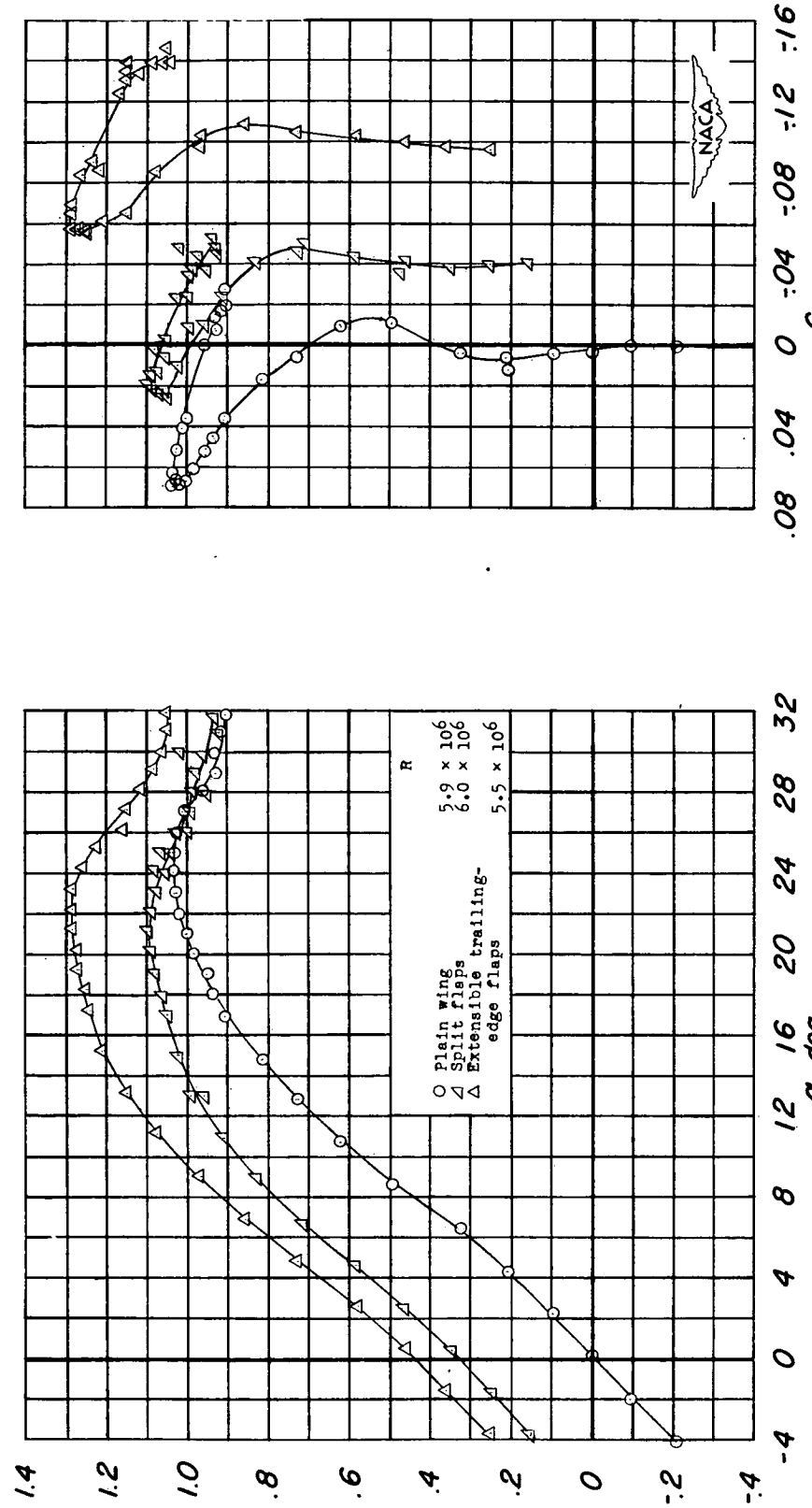

(a) C_L plotted against α and C_m.

Figure 8.- Effect of semispan split and extended trailing-edge flaps deflected 60° on the aerodynamic characteristics of a 52° sweptback wing.

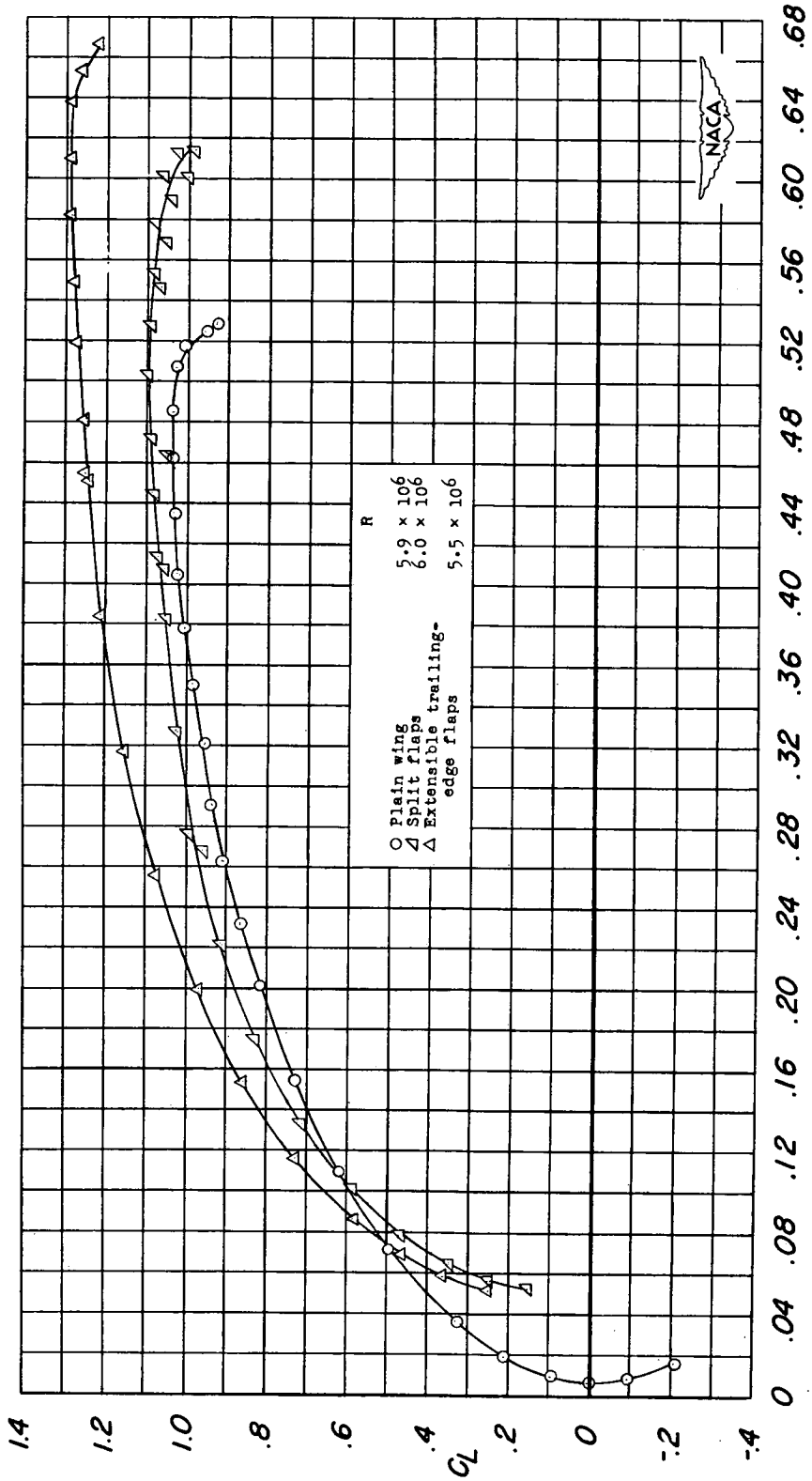

(b) C_L plotted against C_D.

Figure 8.- Concluded.

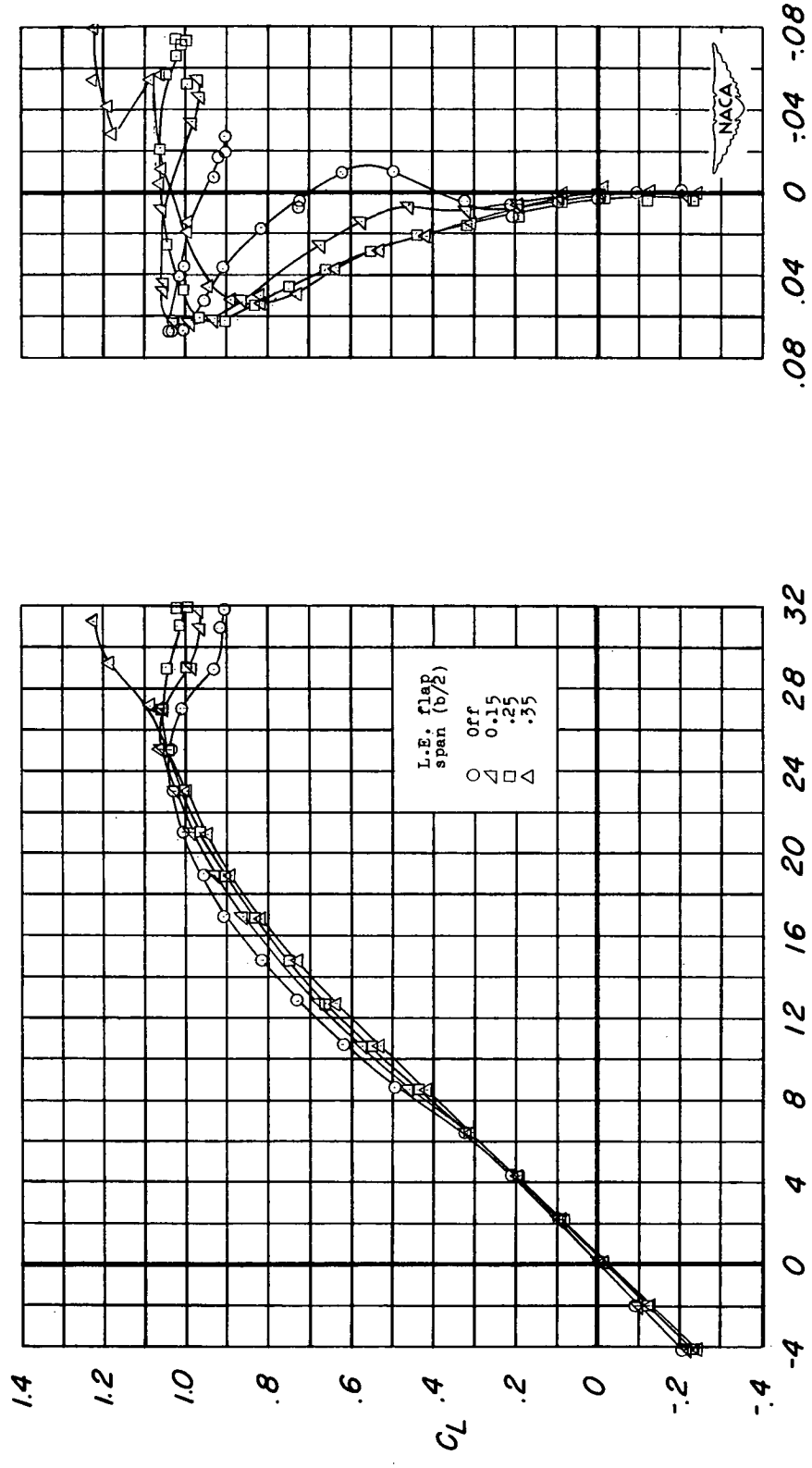

(a) C_L plotted against α and C_m.

Figure 9.- Effect of several spans of extensible leading-edge flaps on the aerodynamic characteristics of a 52° sweptback wing. R = 6.0 × 10^6.

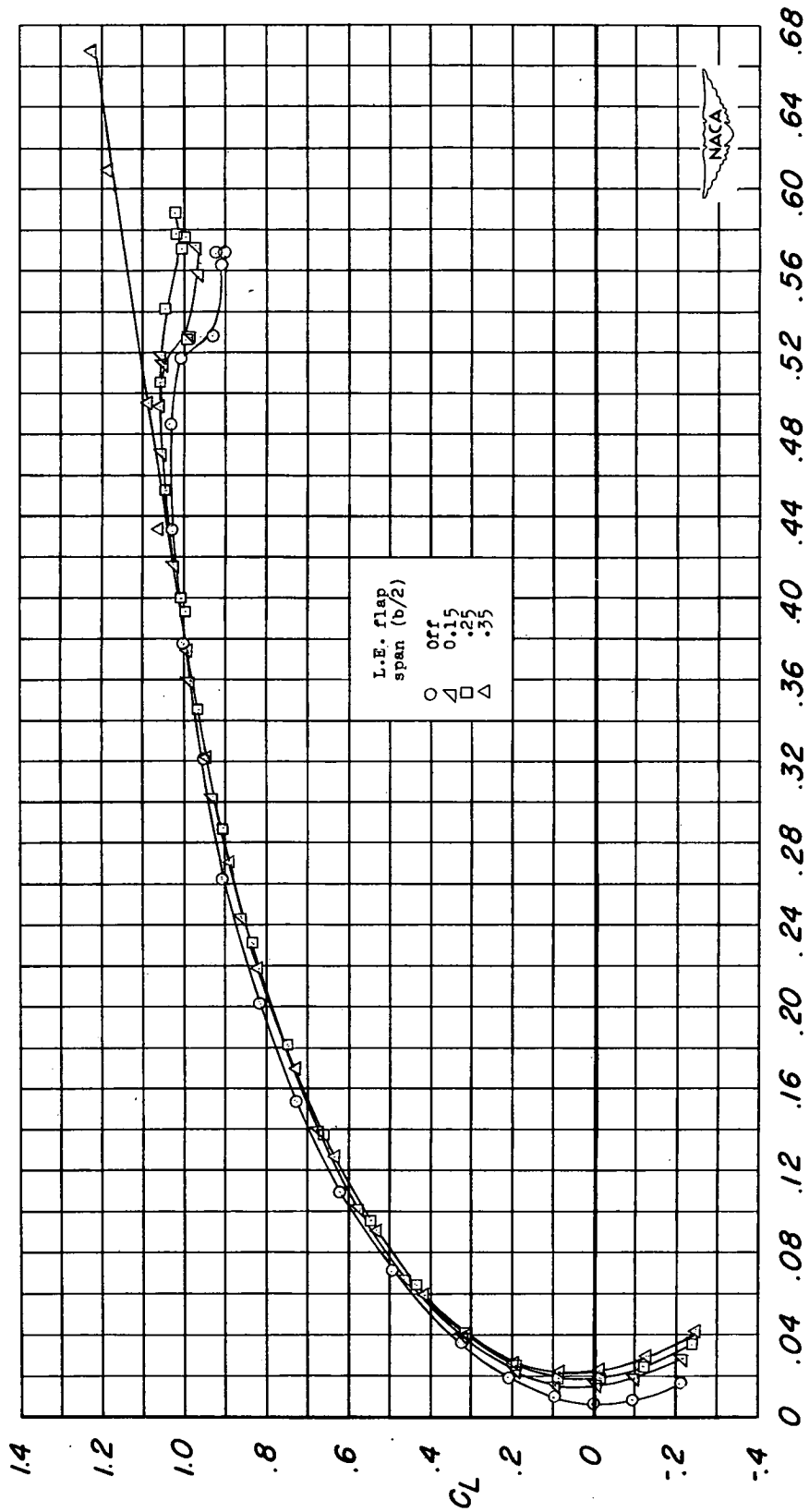

(b) C_L plotted against C_D.

Figure 9.- Concluded.

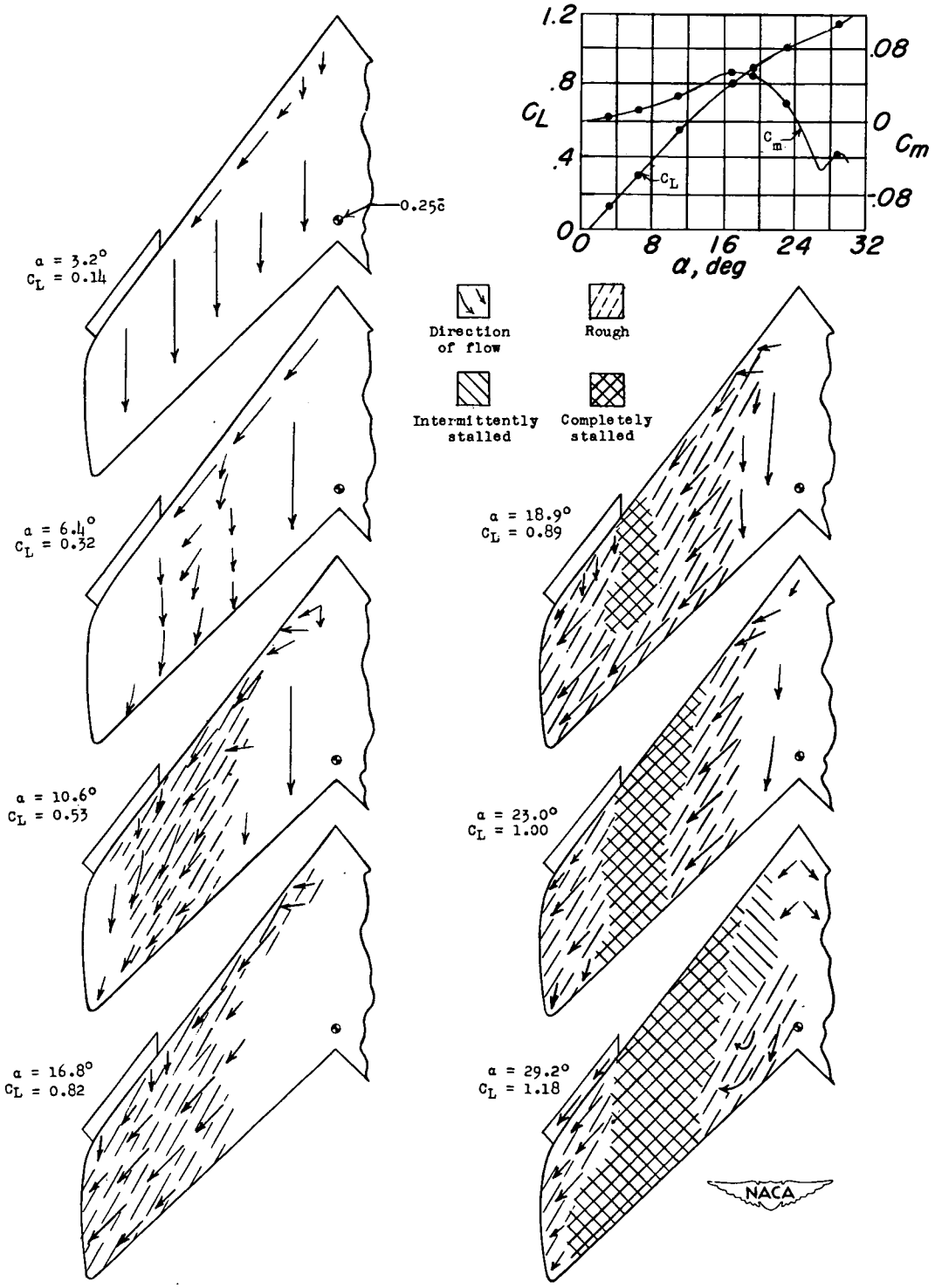

Figure 10.- Stall characteristics of a 52° sweptback wing with 0.35b/2 extensible leading-edge flaps. $R = 5.8 \times 10^6$.

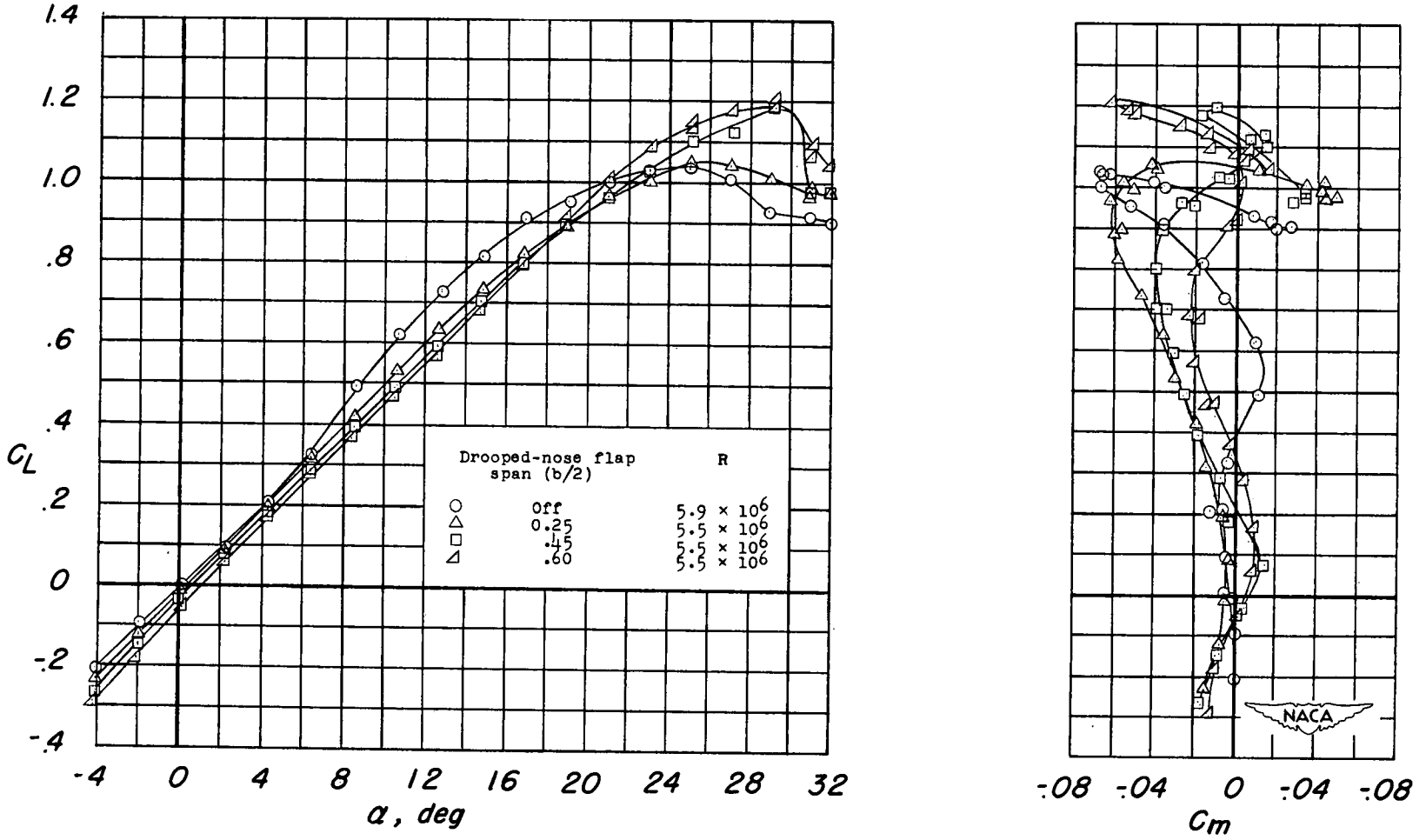

(a) C_L plotted against α and C_m.

Figure 11.- Effect of several spans of drooped-nose flaps deflected 30° on the aerodynamic characteristics of a 52° sweptback wing.

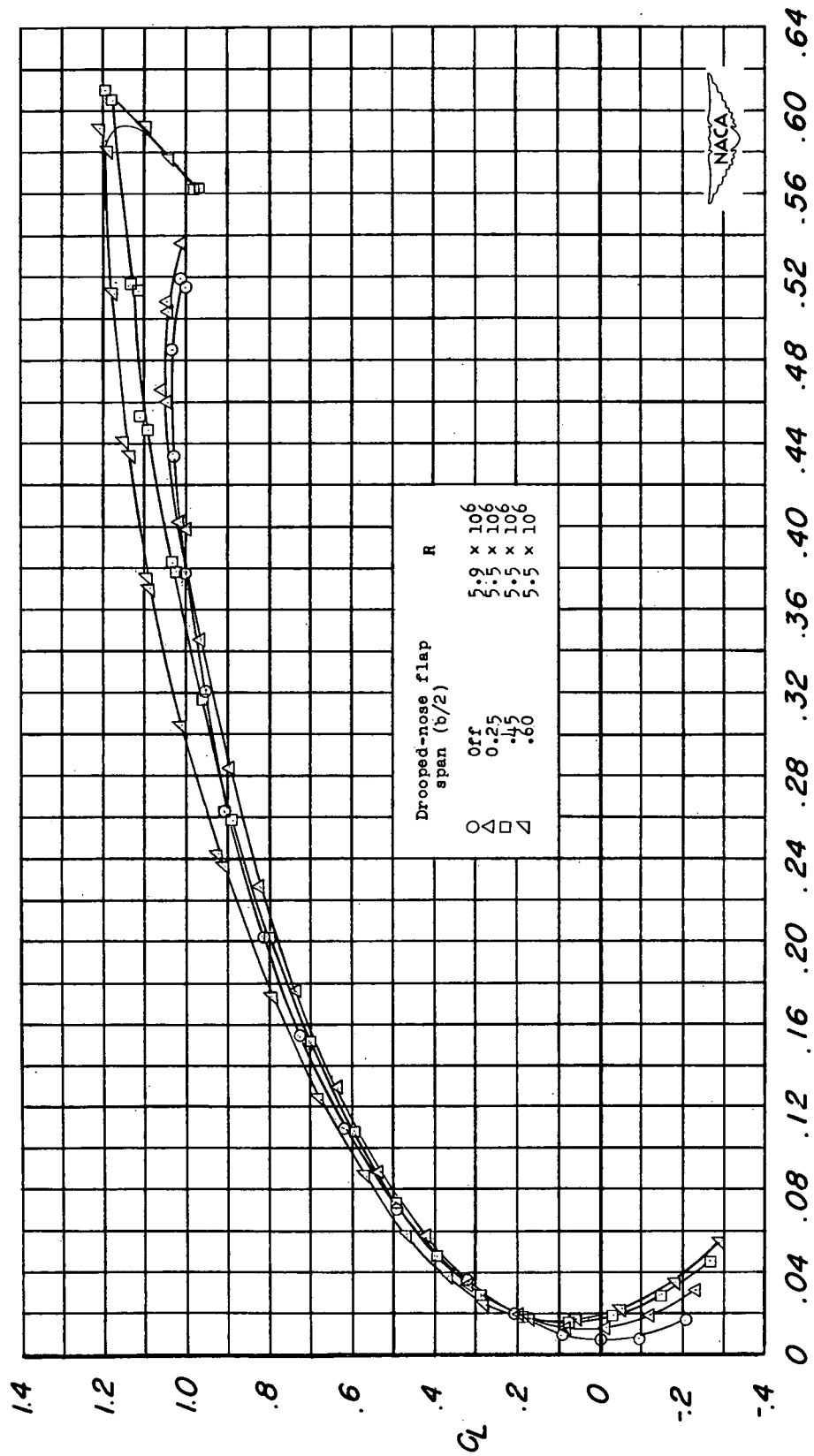

(b) C_L plotted against C_D.

Figure 11.- Concluded.

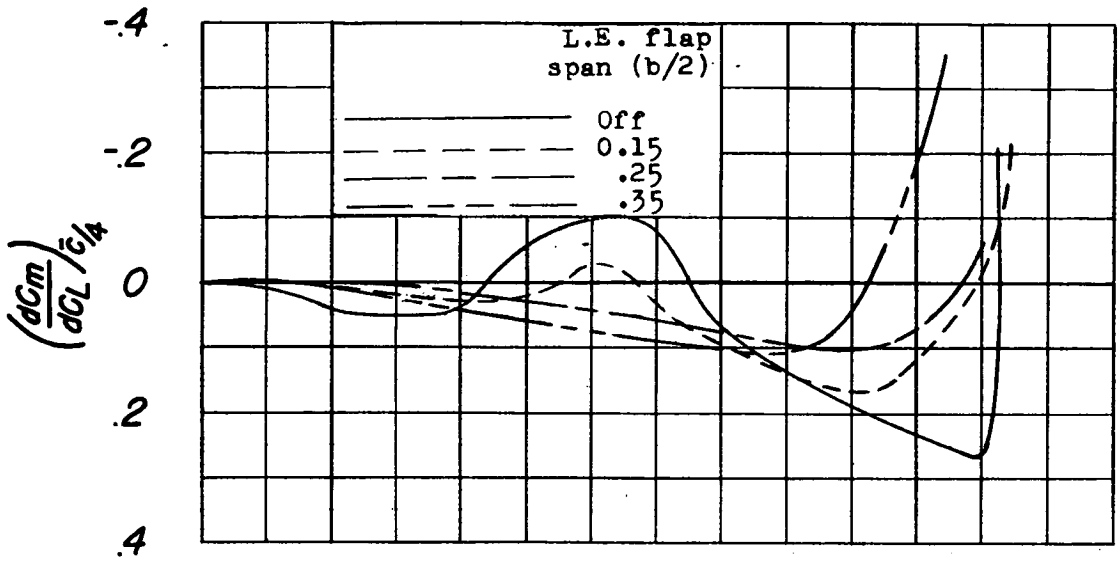

(a) Effect of extensible leading-edge flaps.

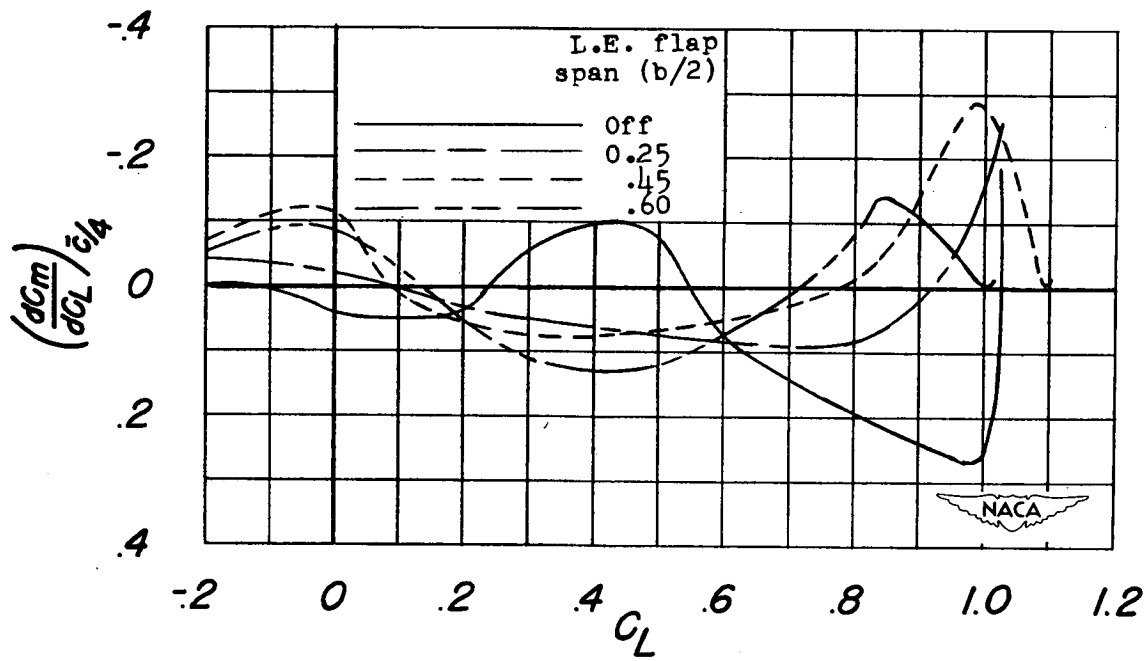

(b) Effect of drooped-nose flaps.

Figure 12.- Variation of $\left(\frac{dC_m}{dC_L}\right)_{\bar{c}/4}$ with lift coefficient of a 52° swept-back wing.

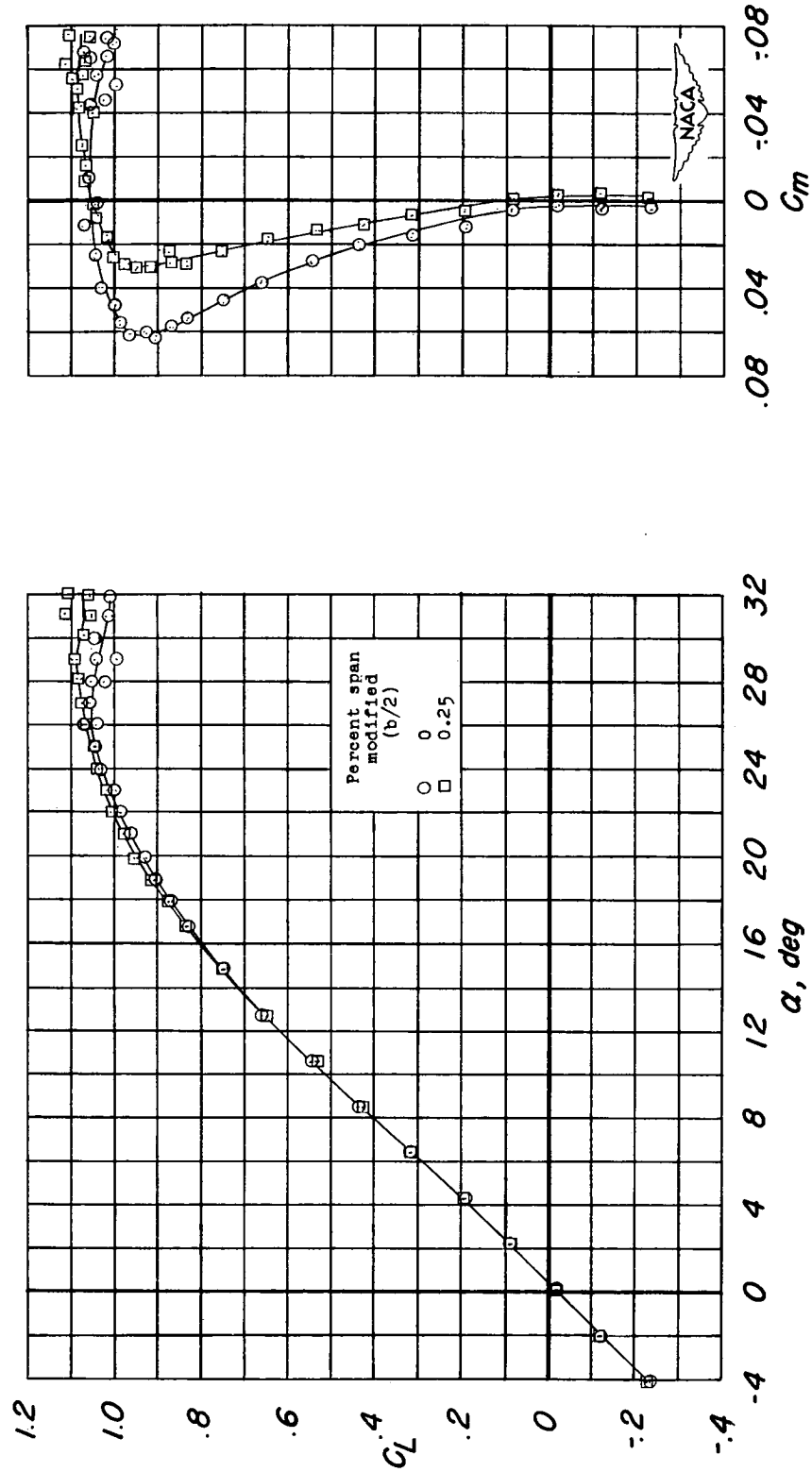

Figure 13.- Effect of rounded leading edge on the aerodynamic characteristics of a 52° sweptback wing with 0.25b/2 extensible leading-edge flaps. $R = 5.5 \times 10^6$.

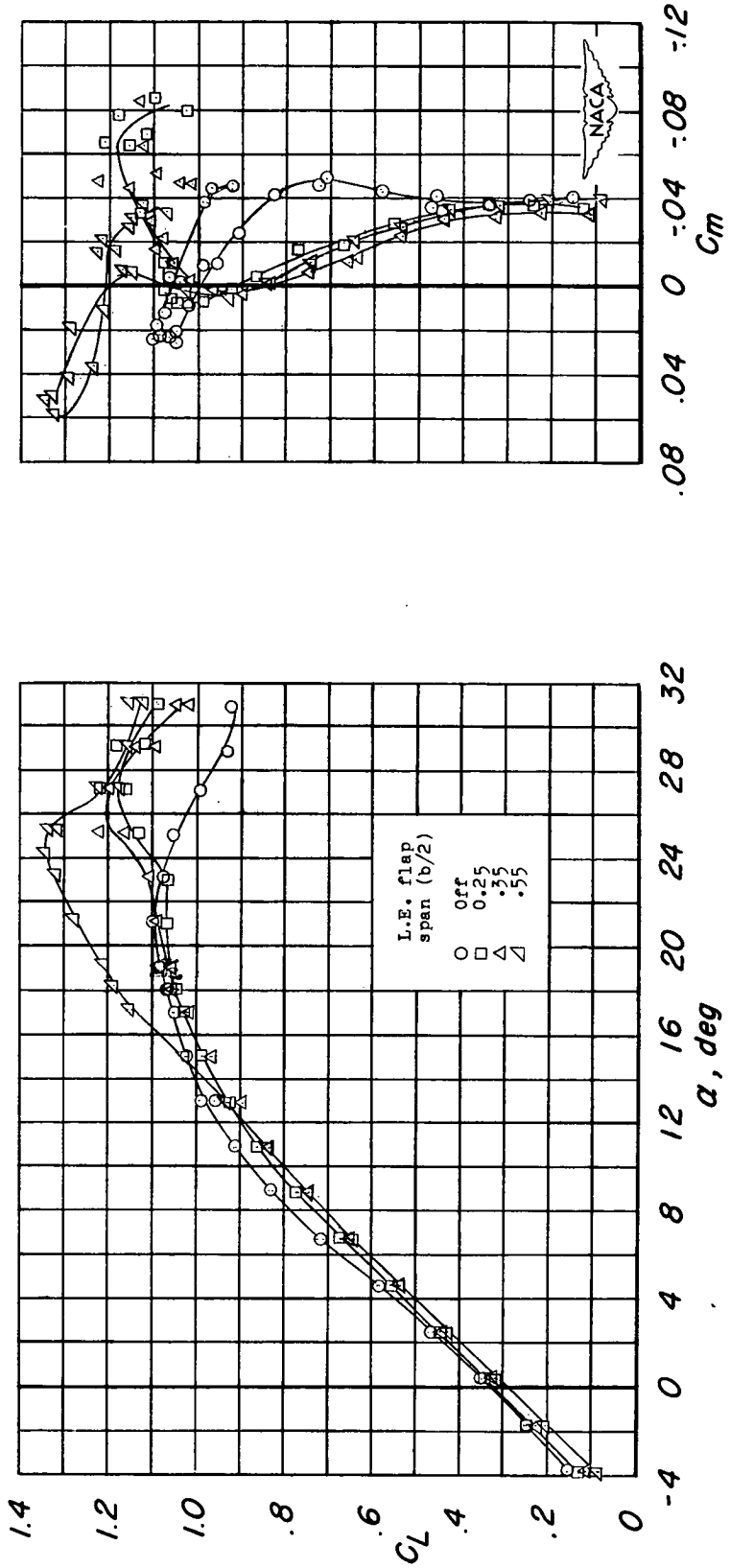

(a) C_L plotted against α and C_m.

Figure 14.- Effect of several spans of extensible leading-edge flaps on the aerodynamic characteristics of a 52° sweptback wing with semispan split flaps deflected 60°. R = 6.0 × 10^6.

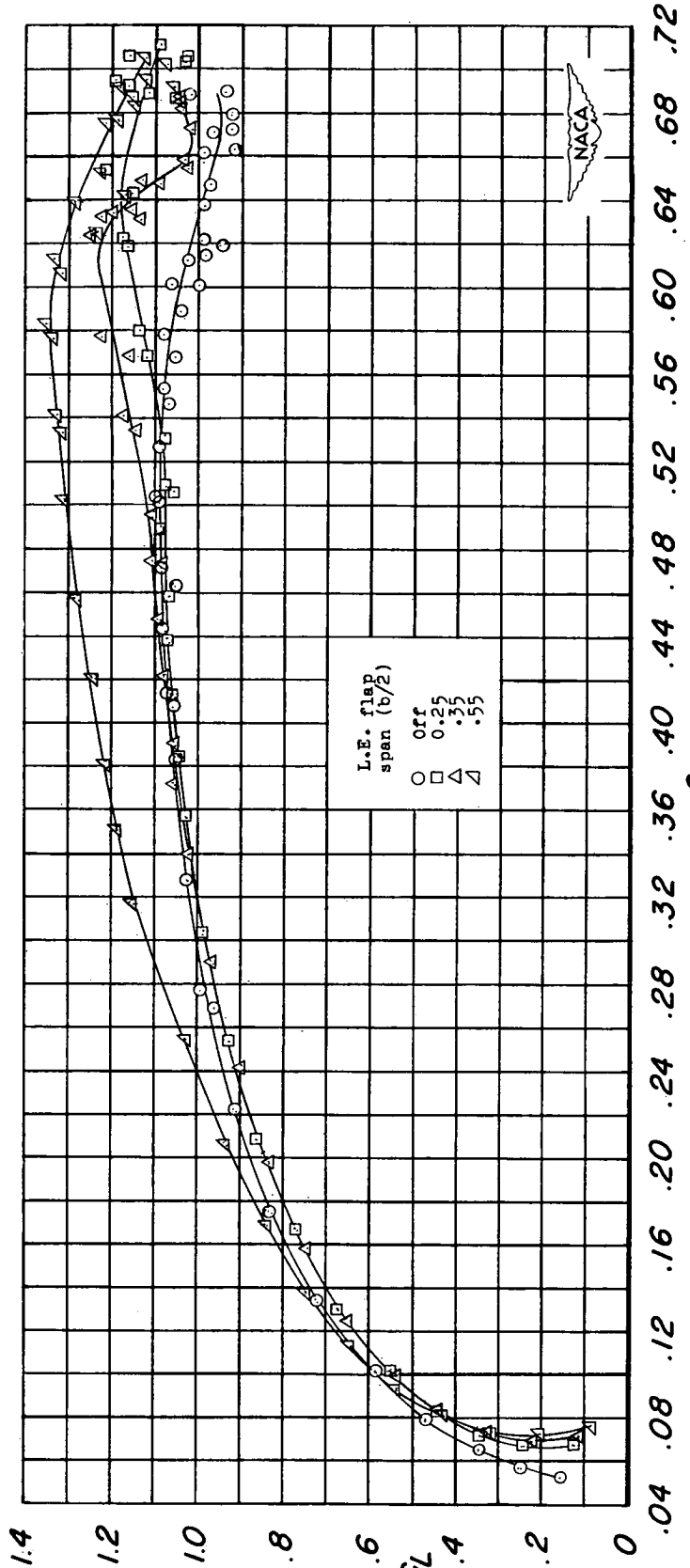

(b) C_L plotted against C_D.

Figure 14.- Concluded.

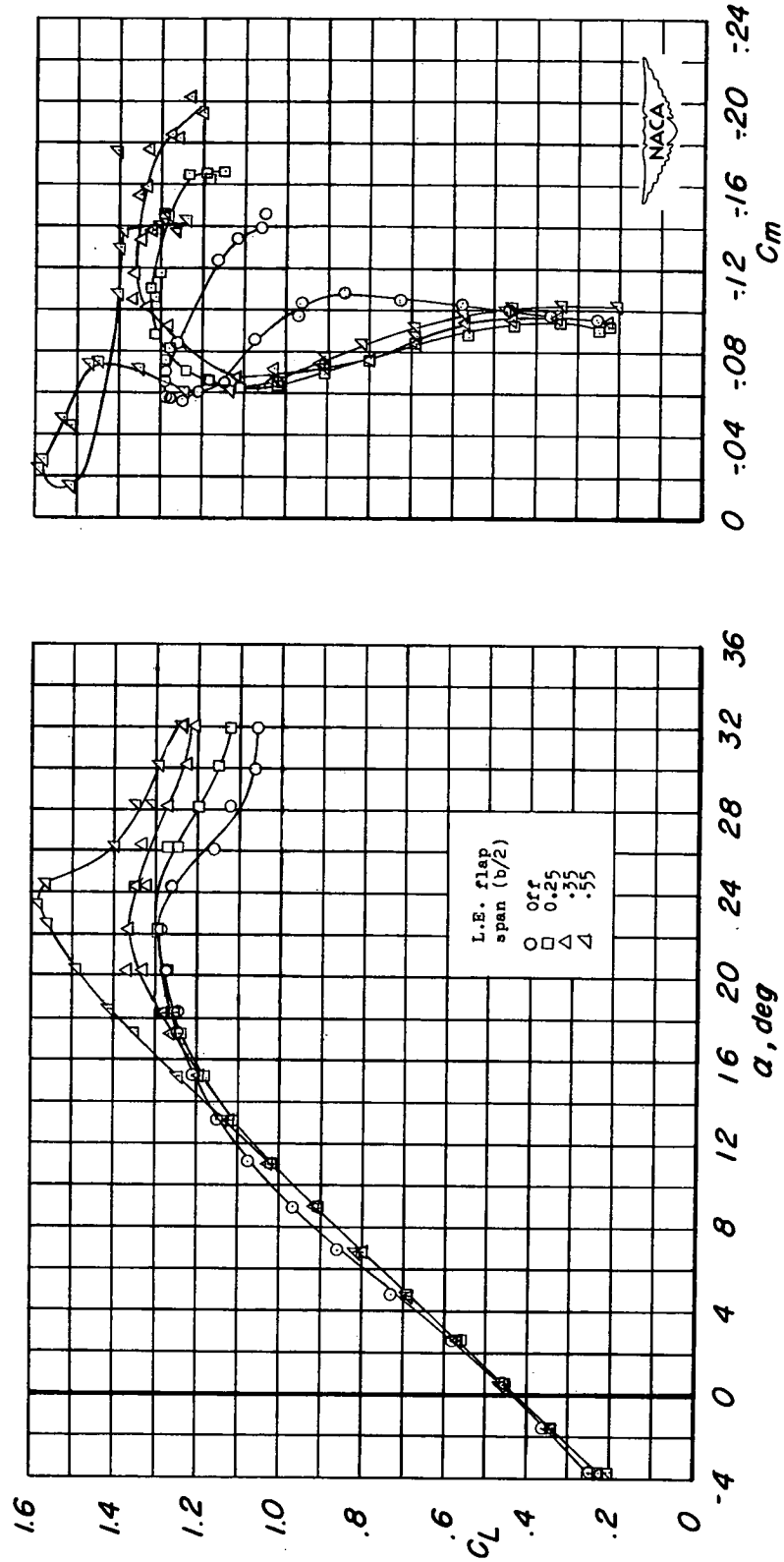

(a) C_L plotted against α and C_m.

Figure 15.- Effect of several spans of extensible leading-edge flaps on the aerodynamic characteristics of a 52° sweptback wing with semispan extended trailing-edge flaps deflected 60°. $R = 5.5 \times 10^6$.

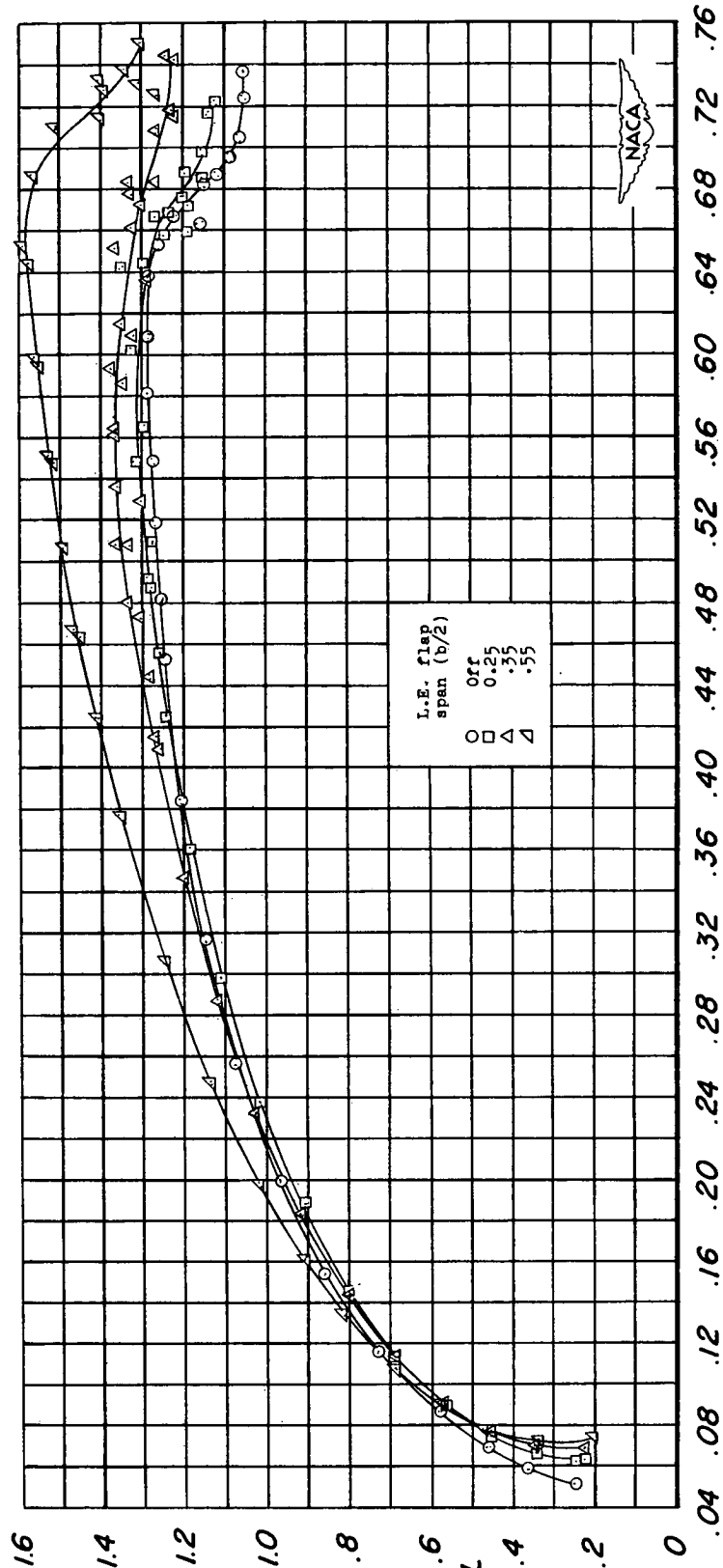

(b) C_L plotted against C_D.

Figure 15.- Concluded.

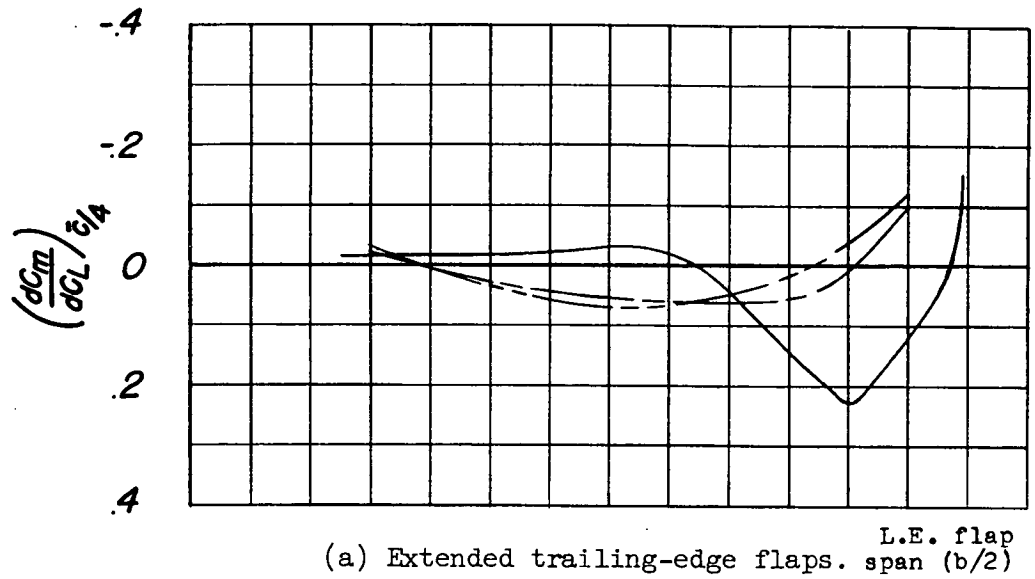

(a) Extended trailing-edge flaps.

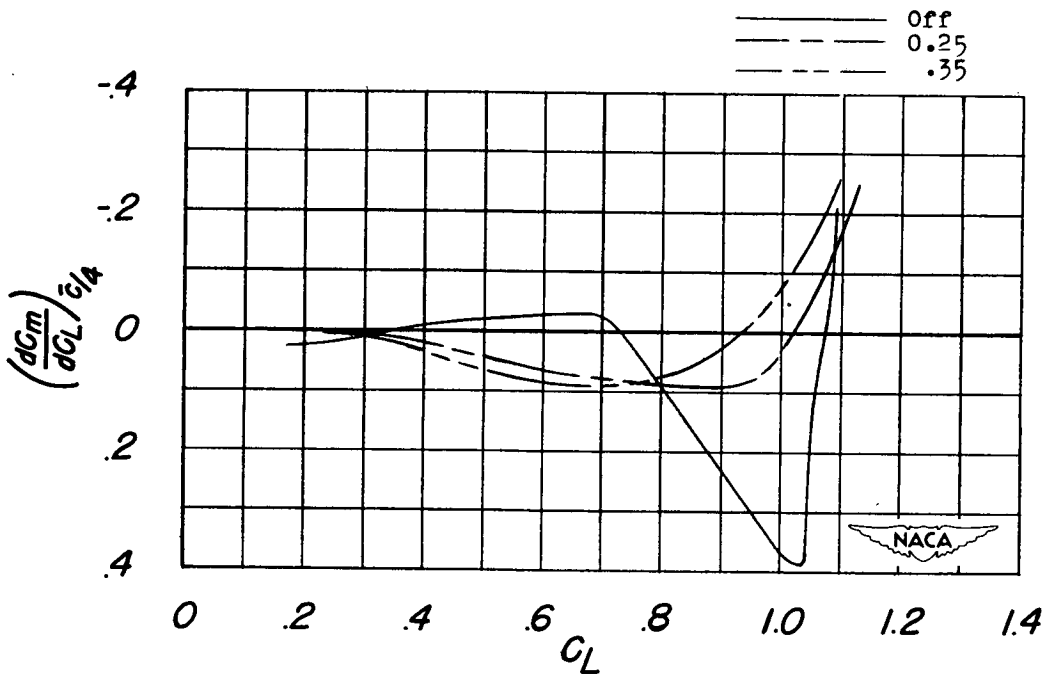

(b) Split flaps.

Figure 16.- Variation of $\left(\frac{dC_m}{dC_L}\right)_{\bar{c}/4}$ with lift coefficient of a 52° swept-back wing with semispan trailing-edge flaps and various spans of extensible leading-edge flaps.

Wing Sweepback	Section	L.E. flap span (b/2)	Reference
52°	circular-arc	0.25	
52°	NACA 64_1-112	.575 fence	5
42°	circular-arc	.695	6

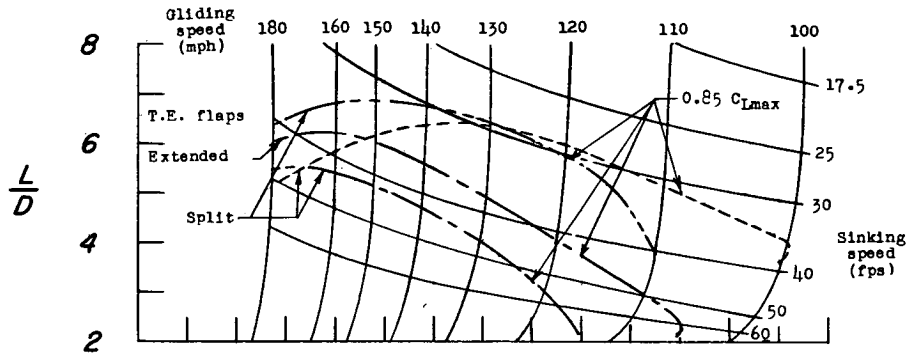

(a) Semispan trailing-edge flaps deflected 60°.

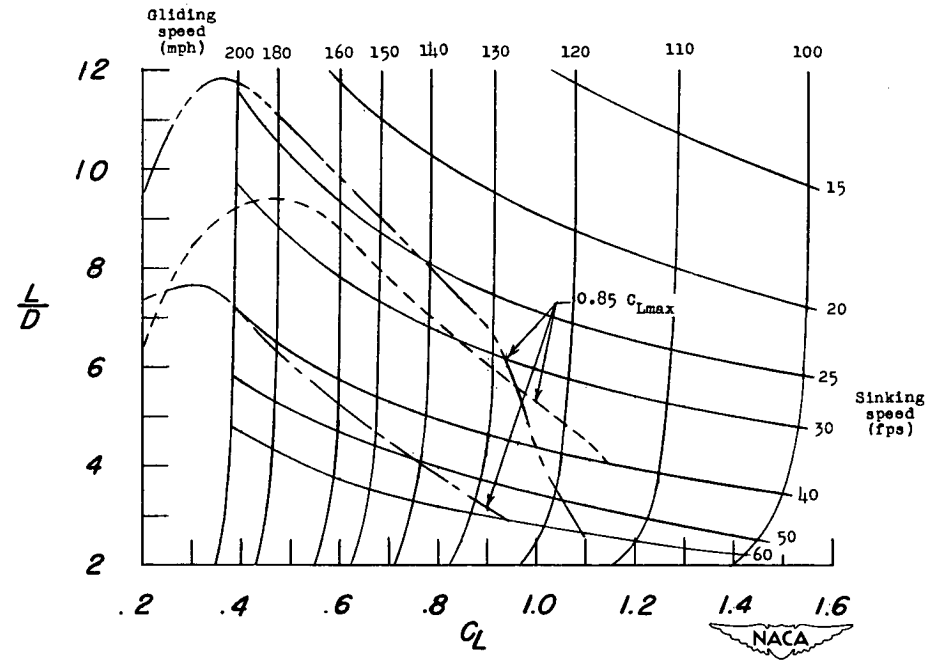

(b) Trailing-edge flaps retracted.

Figure 17.- Comparison of the gliding characteristics of a 52° sweptback circular-arc wing with two other wings. Wing loading, 40 pounds per square foot at sea level.